arXiv:1308.6334v2 [hep-ex] 1 Oct 2013

Heavy Higgs Scalars at Future Hadron Colliders (A Snowmass Whitepaper)

Eric Brownson[1] Nathaniel Craig[2] Ulrich Heintz[3] Gena Kukartsev[3] Meenakshi Narain[3]
Neeti Parashar[4] John Stupak III[4]

[1] University of Puerto Rico, Mayaguez, PR
[2] Rutgers University, Piscataway, NJ
[3] Brown University, Providence, RI
[4] Purdue University Calumet, Hammond, IN

Abstract

We investigate the prospects for discovery or exclusion of additional Higgs scalars at the 14 TeV and 33 TeV LHC in the context of theories with two Higgs doublets. We focus on the modes with the largest production rates at hadron colliders, namely gluon fusion production of a heavy CP-even scalar H or a heavy CP-odd pseudoscalar A. We consider the sensitivity of the decay channels $H \to ZZ \to 4\ell$, and $A \to Zh$ with $Z \to \ell^+\ell^-$ and $h \to b\bar{b}$ or $h \to \tau^+\tau^-$.

1 Introduction

A boson with properties consistent with those predicted for the Standard Model (SM) Higgs boson has been discovered at the LHC [1, 2]. The SM contains the simplest mechanism of spontaneous Electroweak Symmetry Breaking (EWSB) which can give mass to the SM gauge bosons and fermions. However, it is entirely possible that some non-minimal mechanism is responsible for the generation of mass. A large class of non-minimal extensions of the SM Higgs mechanism are described at low energies by a Two Higgs Doublet Model (2HDM) [3, 4], in which there is an additional Higgs doublet relative to the SM Higgs sector. Such a model provides an effective theory description for many natural EWSB extensions, such as the Higgs sector of the Minimal Supersymmetric Standard Model (MSSM) [5, 6], Twin Higgs models [7, 8], and certain classes of Composite Higgs models [9, 10, 11].

In the 2HDM, after EWSB there remain 5 physical Higgs bosons: two CP-even scalars, h and H; one CP-odd pseudoscalar, A; and a charged pair, $H^\pm$. The general parameter space of the 2HDM is vast, but there are several well-motivated asumptions which allow simplification. If, as suggested by the experimenatally observed level of CP violation in nature, the 2HDM is forced to conserve CP at tree level, then after EWSB there are nine free parameters in the scalar potential. A useful basis takes as these nine parameters the four physical Higgs masses, m_h, m_H, m_A, and $m_{H^\pm}$; two angles, α and β; and three couplings, λ_5, λ_6, and λ_7. To simplify the parameter space, the (tree-level) MSSM values of the three scalar couplings are used, $\lambda_5 = \lambda_6 = \lambda_7 = 0$. In addition, the absence of new contributions to tree-level flavor violation may be guaranteed by enforcing discrete symmetries that constrain a given species of right-handed quarks or leptons to couple to only one Higgs doublet in the ultraviolet; this restriction leads to

four types of 2HDM that classify the possible couplings. With this choice, the couplings of each physical Higgs to SM states are determined entirely by the angles α and β, and the type of 2HDM.

Current measurements [12, 13] of the various couplings of the observed Higgs-like state can be used to constrain the allowed parameter space of the 2HDM. Based on such an approach [14, 15, 16, 17], the regions which are allowed at 68% and 95% Confidence Level (CL) are shown in Figure 1 for type I and II 2HDMs (the allowed regions for type III and IV 2HDMs are parametrically similar to type I and type II, respectively). Here the allowed regions of parameter space are shown in terms of the angle β and the combination $\cos(\beta-\alpha)$. In the so-called alignment limit $\cos(\beta-\alpha)\to 0$, the couplings of the light CP-even scalar h become identical to the SM Higgs. Especially in the type II 2HDM, the value of $|\cos(\beta-\alpha)|$ – and hence deviations from SM-like Higgs couplings – is required to be small by the current coupling measurements.

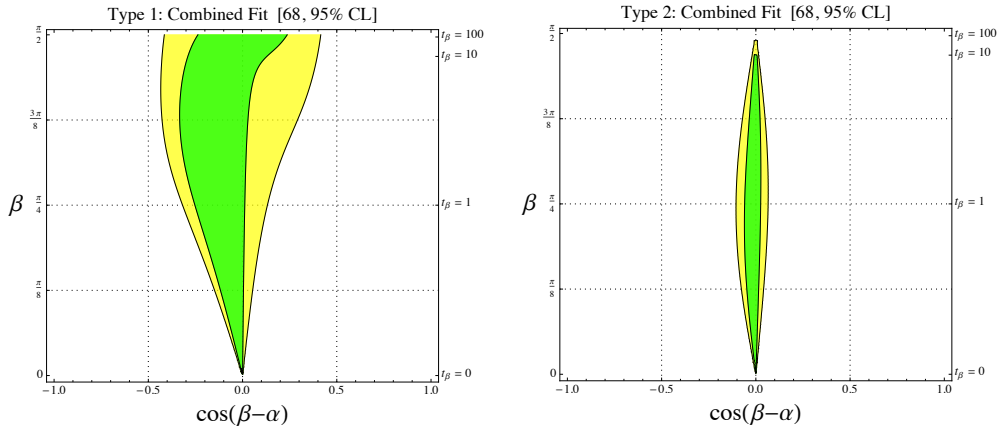


Figure 1: 68% and 95% CL allowed regions of parameter space for type I (left) and type II (right) 2HDMs [14].

2 Background and Signal Simulation

Background Monte Carlo (MC) samples are generated centrally for many common backgrounds [18, 19], for use in a variety of Snowmass studies. Events are generated with MadGraph [20]. Pythia [21] is used for fragmentation and hadronization. Finally, Delphes [22] is used to perform fast detector simulation for a generic "LHC-like" detector [23]. The naming convention used for backgrounds collectively denotes bosons ($W^{\pm}$, Z, γ, and in some samples the SM Higgs boson) by "B". Charged and neutral leptons are collectively denoted by "L". Light quarks and anti-quarks (including bottom) are denoted by "j". The top quark and anti-quark are denoted by "t".

Signal MC is generated using the same processing chain as described for background MC. To efficiently cover the 2HDM parameter space, for each signal mass hypothesis the signal MC is generated for a single benchmark point in α and β, while the signal cross section and branching ratios are calculated analytically as a function of α and β for signal mass hypotheses from 200 GeV to 1 TeV in both type I and II 2HDMs.

The gluon fusion production cross sections at $\sqrt{s}$ =14 and 33 TeV for H and A are computed using `ggh@nnlo` [24] with Standard Model Yukawa couplings and analytically re-weighted using the leading-order dependence on α and β in each 2HDM type. The branching ratios are computed analogously using the procedure outlined in [14] with $\lambda_5 = \lambda_6 = \lambda_7 = 0$. Note that as a result the scalar widths are held fixed in the signal MC for a given signal mass hypothesis, although the physical widths vary across the parameter space of α and β. This approximation is reasonable near the alignment limit where the neutral scalars A and H are narrow and finite width effects play a small role in experimental resolution. The cross section times branching ratio in the $\tan(\beta)$ versus $\cos(\beta - \alpha)$ plane for a 500 GeV H (A) decaying to ZZ (Zh) is shown in Figures 2 and 3.

Unless otherwise noted, all tables and plots in this paper assume a signal cross section for a type II 2HDM with $\cos(\beta - \alpha) = -0.06$ and $\tan(\beta) = 1$. This point in parameter space is allowed by current limits from Higgs coupling measurements. The signal cross section times branching ratio for this benchmark point are given in Tables A.1, A.2, A.3, and A.4. All intermediate results assume branching ratios for $h \to b\bar{b}$ and $\tau^+\tau^-$ of a 125 GeV SM Higgs, but the final results allow these branching ratios to vary across parameter space.

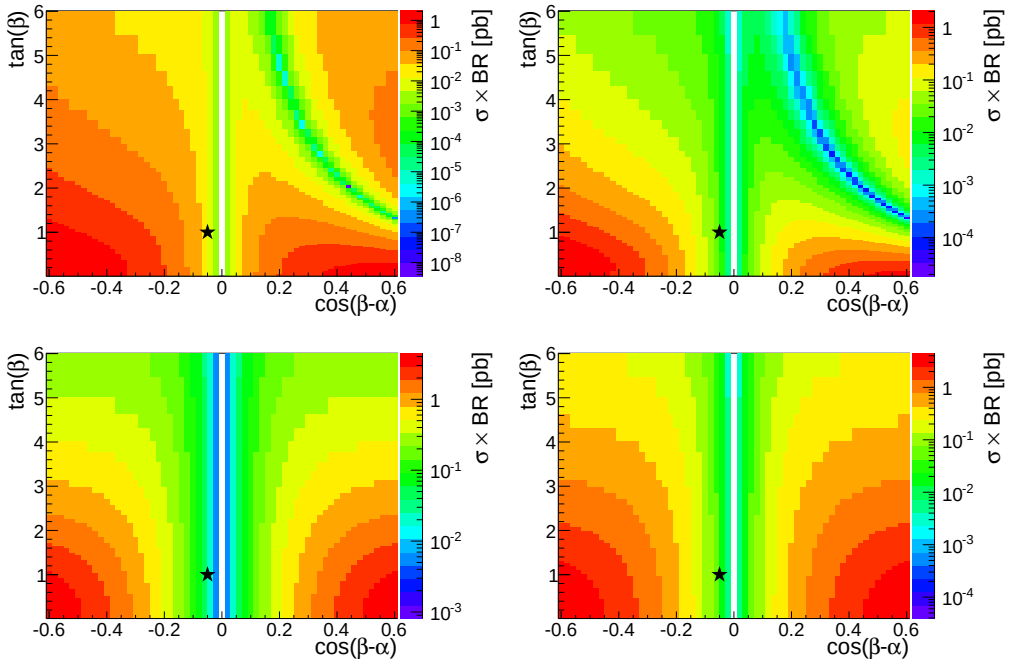


Figure 2: Cross section times branching ratio for $pp \to H \to ZZ$ (top) and $pp \to A \to Zh$ (bottom) at $\sqrt{s} = 14$ TeV in the $\tan(\beta)$ versus $\cos(\beta - \alpha)$ plane, for type I 2HDM (left) and type II 2HDM (right). All plots assume $m(H/A) = 500$ GeV.

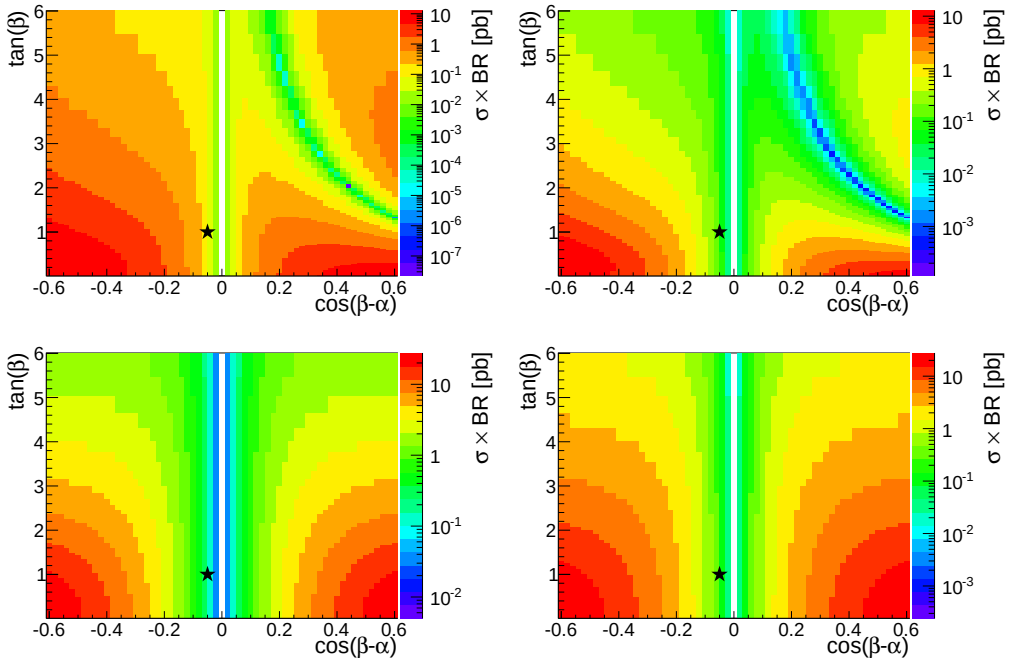


Figure 3: Cross section times branching ratio for $pp \to H \to ZZ$ (top) and $pp \to A \to Zh$ (bottom) at $\sqrt{s} = 33$ TeV in the $\tan(\beta)$ versus $\cos(\beta - \alpha)$ plane, for type I 2HDM (left) and type II 2HDM (right). All plots assume $m(H/A) = 500$ GeV.

3 Analysis

Three scenarios are considered, corresponding to the expectations for LHC Phase I, LHC Phase II (HL-LHC), and HE-LHC running. For LHC Phase I, we assume a total integrated luminosity of $\int Ldt = 300$ fb^{-1} at $\sqrt{s} = 14$ TeV, with an average of 50 pileup interactions per bunch crossing. For the LHC Phase II, we assume a total integrated luminosity of $\int Ldt = 3000$ fb^{-1} at $\sqrt{s} = 14$ TeV, with an average of 140 pileup interactions per bunch crossing. For the HE-LHC, we assume a total integrated luminosity of $\int Ldt = 3000$ fb^{-1} at $\sqrt{s} = 33$ TeV, with an average of 140 pileup interactions per bunch crossing.

For each of these three scenarios, the sensitivity of direct searches for the heavy, neutral Higgses is determined. The sensitivity for H discovery and exclusion are evaluated in the four lepton ($\ell = e, \mu$) final state. The sensitivity for A discovery and exclusion are evaluated in $\ell^+\ell^- bb$ and $\ell^+\ell^-\tau\tau$ final states.

3.1 $H \to ZZ$

The four lepton final state provides the best sensitivity in a search for the CP-even scalar H, due to the low background rate and fully-reconstructible, high-resolution final state. We therefore focus on this decay mode.

The following criteria are applied to leptons:

- $p_T \geq 5$ GeV
- $|\eta| \leq 2.5$
- Relative isolation ≤ 0.1 (after FastJet $\rho \times A$ correction)

Z boson candidates are constructed from pairs of opposite-sign (OS), same-flavor (SF) lepton pairs, with a dilepton invariant mass between 60 GeV and 100 GeV. H candidates are constructed from Z pairs with an invariant mass above 150 GeV.

In order to fire a leptonic trigger, it is assumed that events must contain either a leading lepton with $p_T \geq 30$ GeV, or a leading lepton with $p_T \geq 20$ GeV and a sub-leading lepton with $p_T \geq 10$ GeV. Events are further required to contain exactly four leptons and exactly two Z candidates, one of which must have an invariant mass between 80 GeV and 100 GeV. The signal and background yields at various stages of selection for the 300 fb^{-1} analysis are shown in Tables 1 and 2. Analogous tables for the 3000 fb^{-1} analysis at $\sqrt{s} = 14$ TeV ($\sqrt{s} = 33$ TeV) are shown in Tables 3 and 4 (5 and 6). Various kinematic distributions for selected events are shown in Figures 4 (300 fb^{-1}at $\sqrt{s} = 14$ TeV), 5 (3000 fb^{-1}at $\sqrt{s} = 14$ TeV), and 6 (3000 fb^{-1}at $\sqrt{s} = 33$ TeV).

3.1.1 Results

The distribution of the H candidate invariant mass is used to assess discovery and exclusion potential. A 20% rate uncertainty in the backgrounds is assumed. Figure 7 shows the cross section which can be excluded at 95% CL for each H mass hypothesis, as well as the cross section required for 3σ and 5σ signal significance, at both $\sqrt{s} = 14$ and 33 TeV. Also shown is the cross section for a type II 2HDM with $\cos(\beta-\alpha) = -0.06$ and $\tan(\beta) = 1$.

The cross sections required for exclusion, observation, and discovery are then interpreted in the parameter space of Type I and II 2HDMs. Figure 8 shows the regions in

Signal Mass [GeV]	$N_{lepton} = 4$	Lepton Trigger	$N_Z \geq 1$	$N_Z = 2$	$N_H = 1$
200	1.09e+3	1.09e+3	1.09e+3	1.07e+3	1.07e+3
250	1.24e+3	1.24e+3	1.23e+3	1.21e+3	1.21e+3
300	497	497	496	486	486
350	251	251	251	246	246
400	33	33	33	32.3	32.3
450	18.7	18.7	18.7	18.3	18.3
500	13	13	13	12.8	12.8
600	7.28	7.28	7.27	7.13	7.13
700	4.5	4.5	4.5	4.41	4.41
800	2.97	2.97	2.97	2.91	2.91
900	2	2	2	1.96	1.96
1000	1.34	1.34	1.34	1.32	1.32

Table 1: Expected number of events for the $H \to ZZ$ signal in the four lepton final state for $\int Ldt = 300$ fb^{-1} at $\sqrt{s} = 14$ TeV with $< N_{PU} >= 50$.

Background	$N_{lepton} = 4$	Lepton Trigger	$N_Z \geq 1$	$N_Z = 2$	$N_H = 1$
B, Bj, Bjj-vbf, BB, BBB	5.35e+3	5.35e+3	5.3e+3	4.53e+3	4.53e+3
tj, tB, tt, ttB	475	475	231	29.5	29.5
H	74.1	73.3	69.6	0	0
Total Background	5.9e+3	5.9e+3	5.6e+3	4.56e+3	4.56e+3

Table 2: Expected number of events for the SM backgrounds in the four lepton final state for $\int Ldt = 300$ fb^{-1} at $\sqrt{s} = 14$ TeV with $< N_{PU} >= 50$.

Signal Mass [GeV]	$N_{lepton} = 4$	Lepton Trigger	$N_Z \geq 1$	$N_Z = 2$	$N_H = 1$
200	1.17e+4	1.17e+4	1.17e+4	1.14e+4	1.14e+4
250	1.33e+4	1.33e+4	1.33e+4	1.3e+4	1.3e+4
300	5.29e+3	5.29e+3	5.29e+3	5.17e+3	5.17e+3
350	2.63e+3	2.63e+3	2.62e+3	2.57e+3	2.57e+3
400	343	343	342	335	335
450	196	196	195	192	192
500	135	135	135	132	132
600	74.2	74.2	74.1	72.7	72.7
700	46.4	46.4	46.3	45.4	45.4
800	30.4	30.4	30.4	29.8	29.8
900	20.4	20.4	20.4	20	20
1000	13.8	13.8	13.8	13.6	13.6

Table 3: Expected number of events for the $H \to ZZ$ signal in the four lepton final state for $\int Ldt = 3000$ fb^{-1} at $\sqrt{s} = 14$ TeV with $< N_{PU} >= 140$.

Background	$N_{lepton} = 4$	Lepton Trigger	$N_Z \geq 1$	$N_Z = 2$	$N_H = 1$
B, Bj, Bjj-vbf, BB, BBB	5.65e+4	5.64e+4	5.58e+4	4.77e+4	4.77e+4
tj, tB, tt, ttB	1.54e+4	1.53e+4	5.47e+3	336	336
H	874	865	813	0	0
Total Background	7.27e+4	7.26e+4	6.21e+4	4.8e+4	4.8e+4

Table 4: Expected number of events for the SM backgrounds in the four lepton final state for $\int Ldt = 3000$ fb^{-1} at $\sqrt{s} = 14$ TeV with $< N_{PU} >= 140$.

Signal Mass [GeV]	$N_{lepton} = 4$	Lepton Trigger	$N_Z \geq 1$	$N_Z = 2$	$N_H = 1$
200	4.17e+4	4.17e+4	4.16e+4	4.07e+4	4.07e+4
250	5.14e+4	5.14e+4	5.13e+4	5.03e+4	5.03e+4
300	2.14e+4	2.14e+4	2.14e+4	2.09e+4	2.09e+4
350	1.15e+4	1.15e+4	1.14e+4	1.12e+4	1.12e+4
400	1.6e+3	1.6e+3	1.6e+3	1.57e+3	1.57e+3
450	973	973	971	950	950
500	699	699	698	683	683
600	435	435	435	426	426
700	303	303	302	296	296
800	217	217	217	212	212
900	159	159	159	155	155
1000	118	118	118	115	115

Table 5: Expected number of events for the $H \to ZZ$ signal in the four lepton final state for $\int Ldt = 3000$ fb^{-1} at $\sqrt{s} = 33$ TeV with $< N_{PU} >= 140$.

Background	$N_{lepton} = 4$	Lepton Trigger	$N_Z \geq 1$	$N_Z = 2$	$N_H = 1$
B, Bj, Bjj-vbf, BB, BBB	1.45e+5	1.45e+5	1.41e+5	1.14e+5	1.14e+5
tj, tB, tt, ttB	1.63e+5	1.61e+5	4.99e+4	2.97e+3	2.97e+3
H	3.58e+3	3.55e+3	3.32e+3	0	0
Total Background	3.11e+5	3.1e+5	1.94e+5	1.17e+5	1.17e+5

Table 6: Expected number of events for the SM backgrounds in the four lepton final state for $\int Ldt = 3000$ fb^{-1} at $\sqrt{s} = 33$ TeV with $< N_{PU} >= 140$.

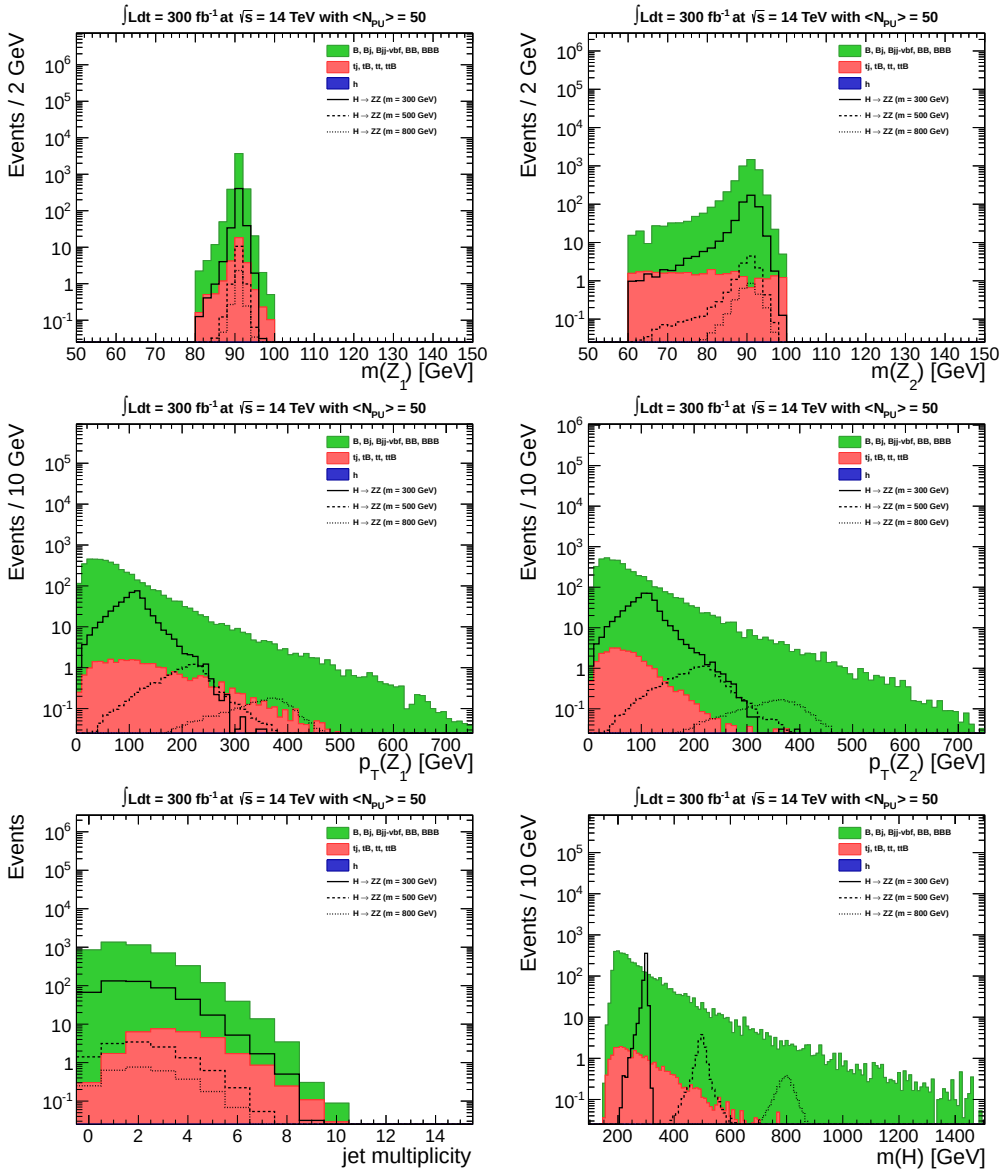


Figure 4: Kinematic distributions for selected events in $\int Ldt = 300$ fb^{-1} at $\sqrt{s} = 14$ TeV with $< N_{PU} >= 50$.

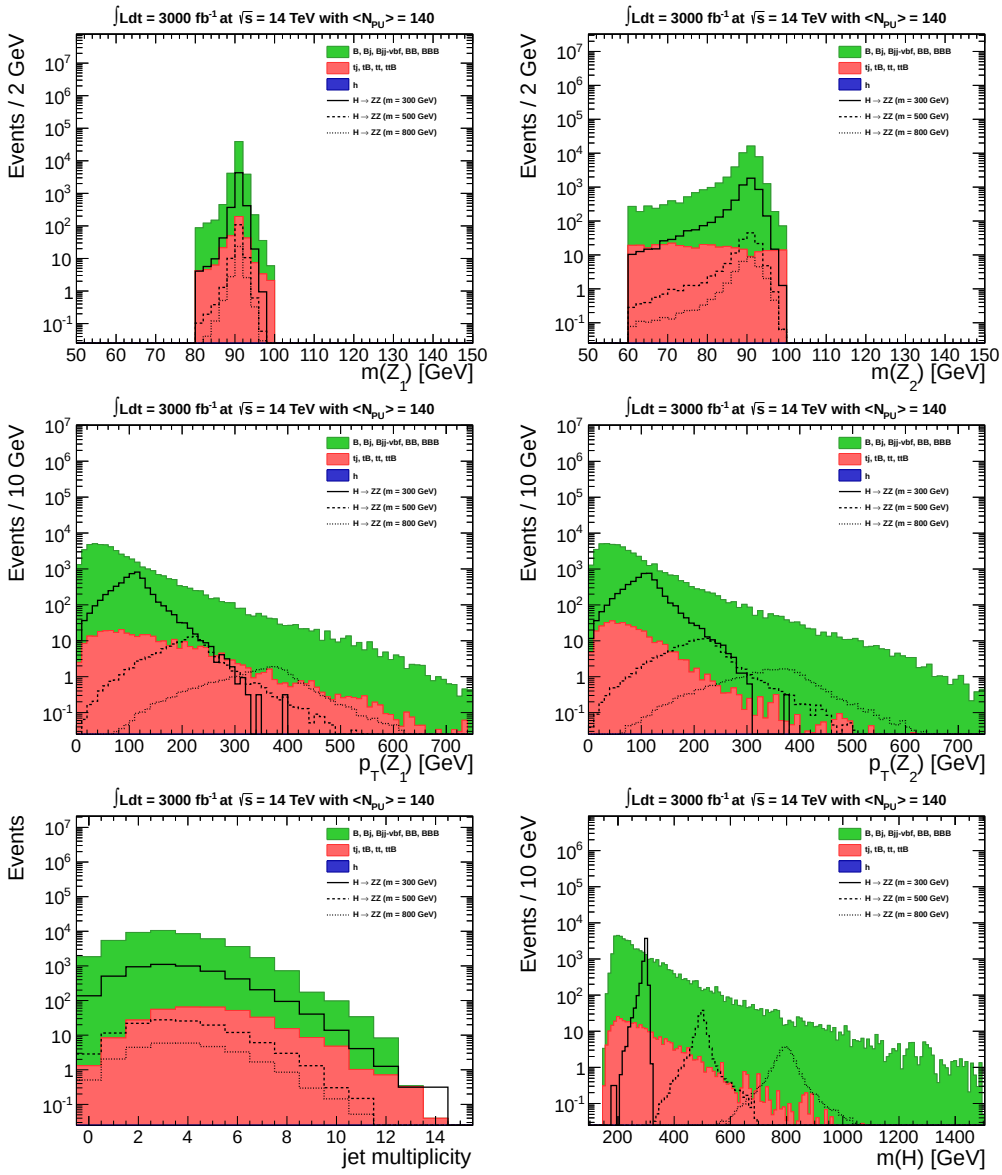


Figure 5: Kinematic distributions for selected events in $\int Ldt = 3000$ fb^{-1} at $\sqrt{s} = 14$ TeV with $< N_{PU} >= 140$.

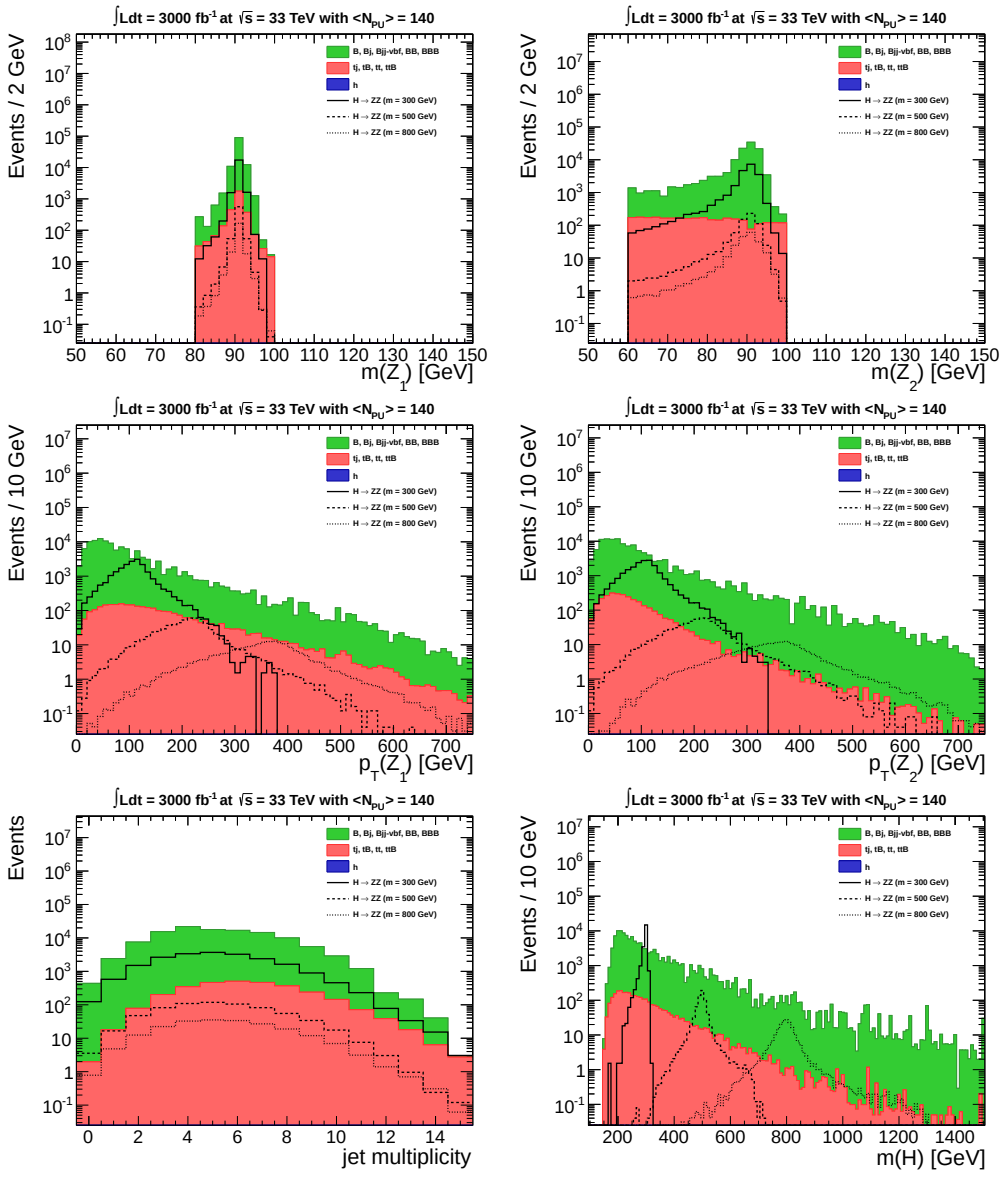


Figure 6: Kinematic distributions for selected events in $\int Ldt = 3000$ fb^{-1} at $\sqrt{s} = 33$ TeV with $< N_{PU} >= 140$.

the $\tan\beta$ versus $\cos(\beta-\alpha)$ plane which can be excluded at 95% CL for the three scenarios under consideration. Figures 9 and 10 show the regions for which 3σ and 5σ signal significance can be obtained. These plots also show the complementarity between direct searches for an extended Higgs sector and precision Higgs coupling measurements using the LHC Higgs coupling projections of [25]. There is a considerable region that can only be excluded through direct search, and also regions where coupling measurements are stronger. In particular, the direct search limits weaken only at large $\tan\beta$ where the production cross section for H falls due to diminishing coupling to the top quark, as well as close to the alignment limit $|\cos(\beta-\alpha)| \to 0$ where the branching ratio for $H \to ZZ$ vanishes.

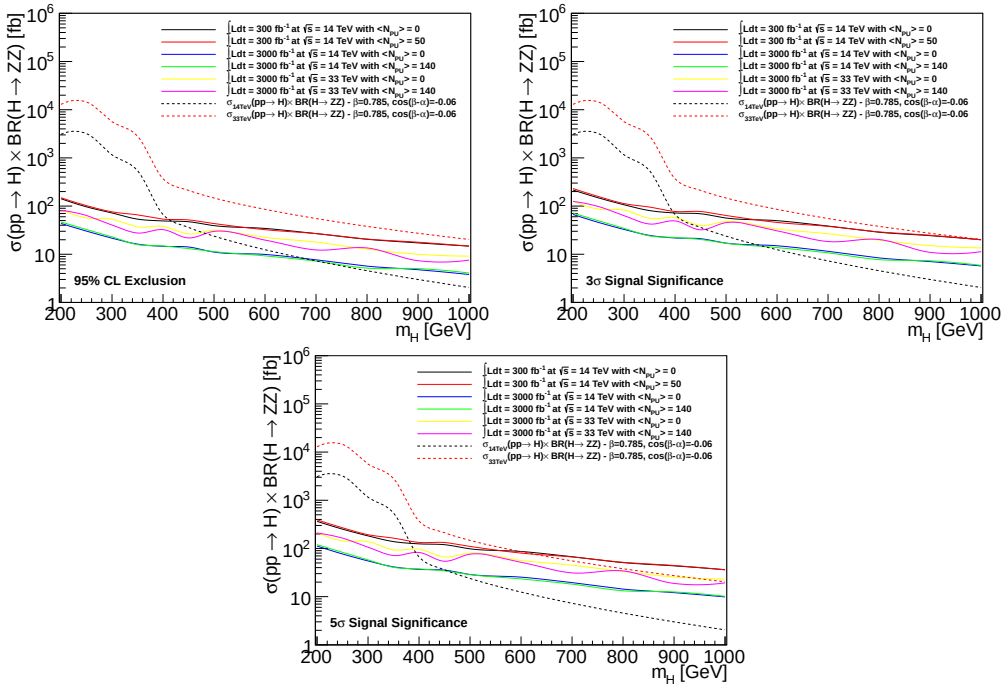


Figure 7: The cross section which can be excluded at 95% CL, and the cross section required for a 3σ and 5σ signal significance, for each H mass hypothesis.

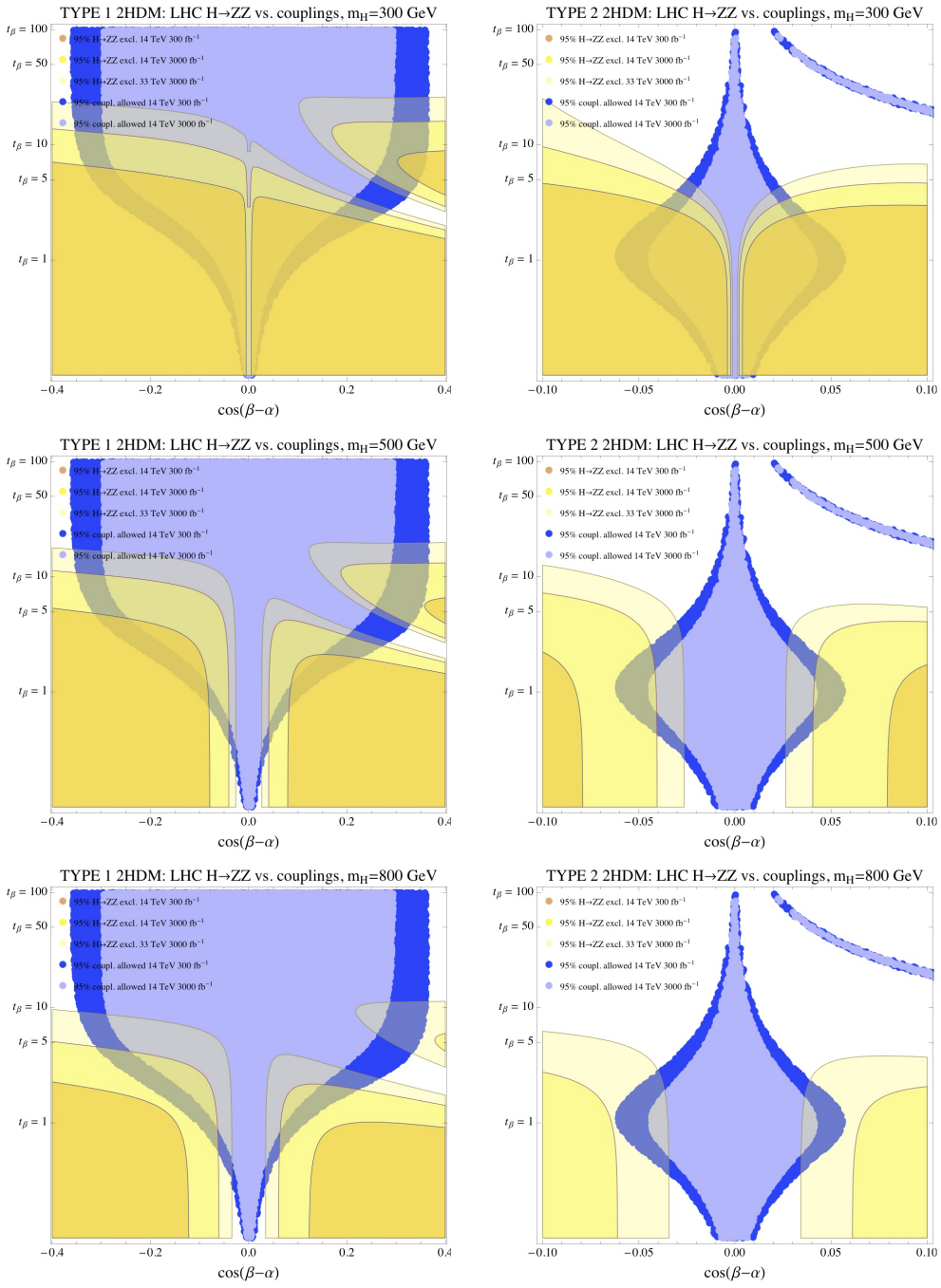


Figure 8: The region of parameter space which could be excluded at 95% CL for various H mass hypotheses in a type I (left) and type II (right) 2HDM. The dark yellow region corresponds to 300 fb^{-1} at $\sqrt{s} = 14$ TeV, the yellow region to 3000 fb^{-1} at $\sqrt{s} = 14$ TeV, and the light yellow region to 3000 fb^{-1} at $\sqrt{s} = 33$ TeV. The region which would remain allowed at 95% CL based on non-observation of deviations from the SM in precision Higgs coupling measurements is shown in dark (light) blue for 300 fb^{-1} (3000 fb^{-1}) [25].

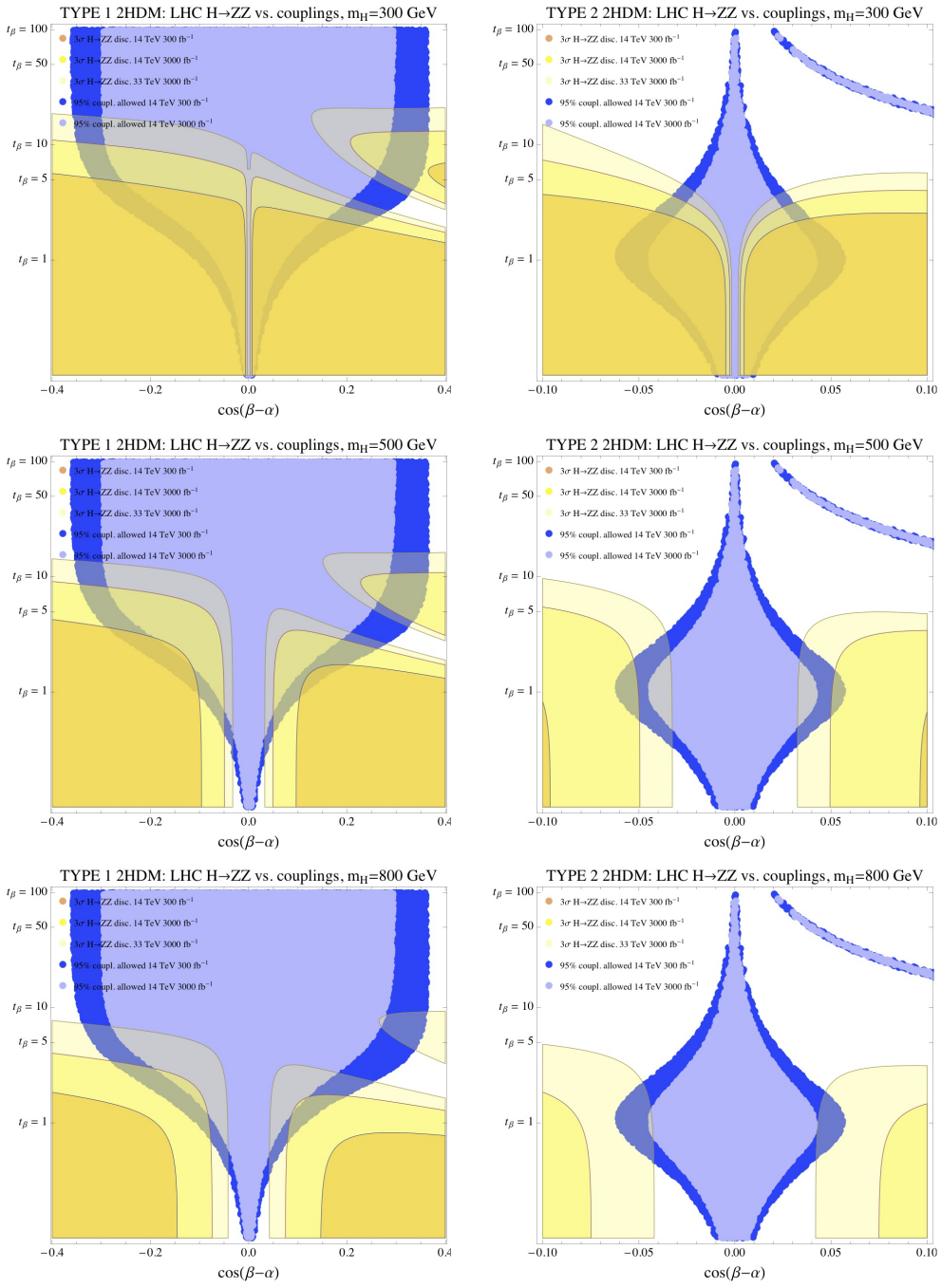


Figure 9: The region of parameter space for which a 3σ signal significance could be obtained for various H mass hypotheses in a type I (left) and type II (right) 2HDM. The dark yellow region corresponds to 300 fb^{-1} at $\sqrt{s} = 14$ TeV, the yellow region to 3000 fb^{-1} at $\sqrt{s} = 14$ TeV, and the light yellow region to 3000 fb^{-1} at $\sqrt{s} = 33$ TeV. The region which would remain allowed at 95% CL based on non-observation of deviations from the SM in precision Higgs coupling measurements is shown in dark (light) blue for 300 fb^{-1} (3000 fb^{-1}) [25].

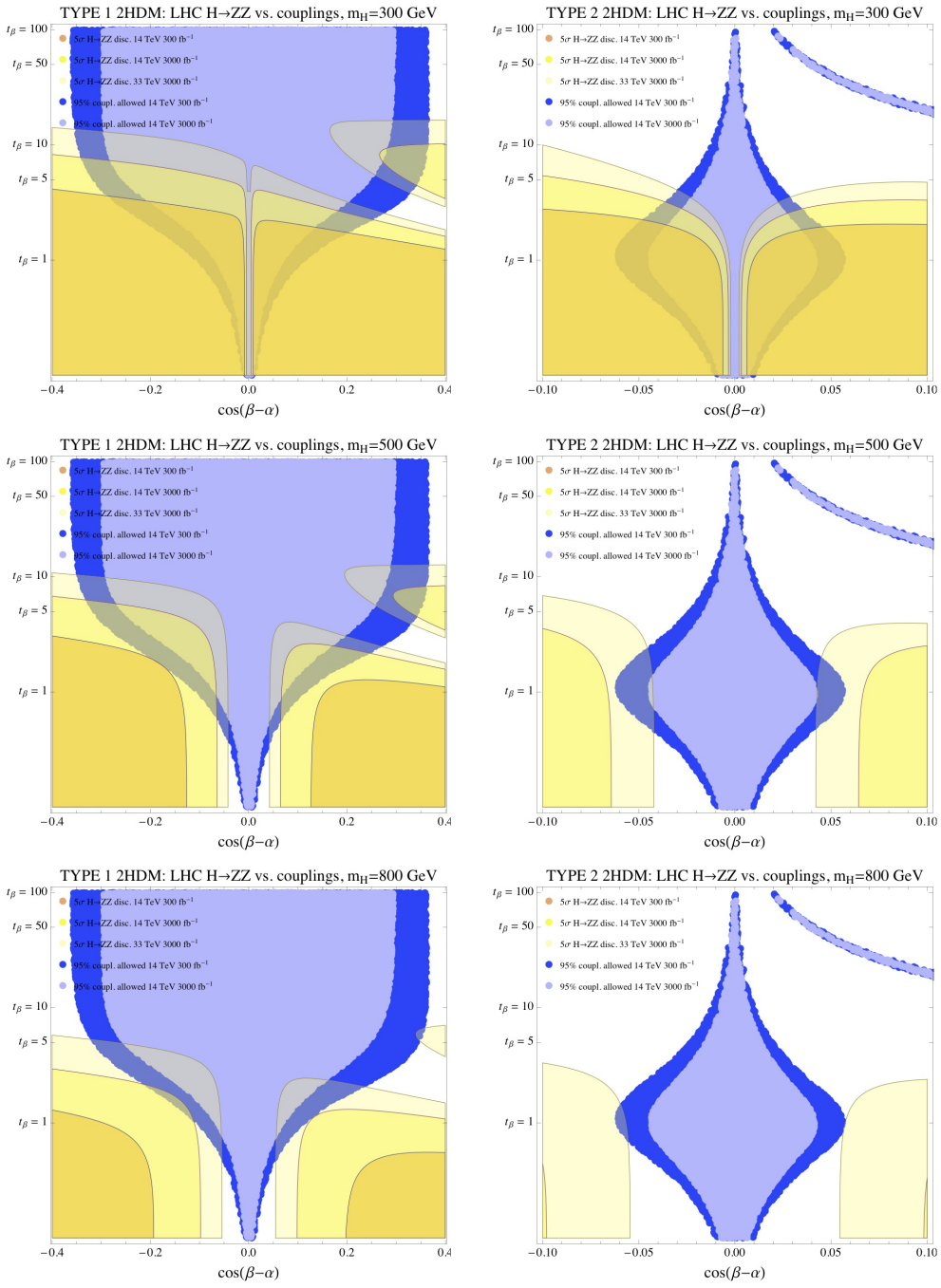


Figure 10: The region of parameter space for which a 5σ signal significance could be obtained for various H mass hypotheses in a type I (left) and type II (right) 2HDM. The dark yellow region corresponds to 300 fb^{-1} at $\sqrt{s} = 14$ TeV, the yellow region to 3000 fb^{-1} at $\sqrt{s} = 14$ TeV, and the light yellow region to 3000 fb^{-1} at $\sqrt{s} = 33$ TeV. The region which would remain allowed at 95% CL based on non-observation of deviations from the SM in precision Higgs coupling measurements is shown in dark (light) blue for 300 fb^{-1} (3000 fb^{-1}) [25].

3.2 $A \to Zh$

A heavy CP-odd pseudo-scalar A cannot decay to ZZ pairs, but often possesses a large width for decay to the distinctive Zh final state. Therefore, the $A \to Zh$ decay mode is the most promising channel for exclusion or discovery in a broad region of parameter space, and we choose to focus on this decay mode with subsequent $Z \to \ell^+\ell^-$ and $h \to b\bar{b}$ or $h \to \tau^+\tau^-$ decays.

The following criteria are applied to leptons:

- $p_T \geq 5$ GeV
- $|\eta| \leq 2.5$
- Relative isolation ≤ 0.1 (after FastJet $\rho \times A$ correction)

The following criteria are applied to b-jets and τ leptons:

- $p_T \geq 20$ GeV
- $|\eta| \leq 2.5$

The tight b-tagging working point [23] is used to identify jets originating from b quarks. This working point assumes a p_T- and η-dependent b-tagging efficiency, which peaks at 70% (60%) for high-p_T jets with $|\eta| \leq 1.2$ ($|\eta| > 1.2$). The mistag rate for c quarks is similarly p_T- and η-dependent, peaking at ∼19%. The mistag rate for light quarks and gluons is a flat 0.01%. The τ-tagging working point assumes a flat 65% (0.4%) efficiency (mis-tag rate).

A pre-selection is applied to select events with a topology consistent with signal events. Events are required to contain exactly two leptons. In order to fire a leptonic trigger, it is assumed that the leading lepton must satisfy $p_T \geq 30$ GeV, or the leading lepton must satisfy $p_T \geq 20$ GeV and the sub-leading lepton must satisfy $p_T \geq 10$ GeV. In the bb channel, events are required to contain exactly two b-jets and fewer than two τ leptons (to maintain orthogonality with the $\tau\tau$ channel). Similarly, in the $\tau\tau$ channel, events are required to contain exactly two τ leptons and fewer than two b-jets. In both channels, events are required to contain exactly one Z boson candidate, constructed from an OS SF lepton pair with an invariant mass satisfying $80 \leq m_{\ell\ell} \leq 100$. Events must also contain exactly one SM Higgs candidate. In the bb channel, Higgs candidates are constructed from a bb pair with an invariant mass satisfying $90 \leq m_{bb} \leq 150$. In the $\tau\tau$ channel, Higgs candidates are constructed from a $\tau\tau$ pair with a visible mass satisfying $55 \leq m_{\tau\tau} \leq 125$. Finally, events must contain an A candidate, constructed from the Z and h candidates, with an invariant mass $m_A \geq 150$ GeV. Pre-selected event yields for 300 fb^{-1}at $\sqrt{s} = 14$ TeV (3000 fb^{-1}at $\sqrt{s} = 33$ TeV) in the bb channel are shown in Tables 7 and 8 (9 and 10). Analogous tables for the $\tau\tau$ channel are shown in Tables A.5 and A.6 (A.7 and A.8). Several kinematic distributions of interest for the 300 fb^{-1}analysis at $\sqrt{s} = 14$ TeV are shown in Figures 11 and A.1 for the bb and $\tau\tau$ channels, respectively. Analogous plots for the 3000 fb^{-1}analysis at $\sqrt{s} = 33$ TeV are shown in Figures 12 and A.2.

Several variables are found to discriminate between pre-selected signal and background events. The three variables which discriminate most strongly are chosen, and cut thresholds are varied simultaneously to determine the set which maximizes signal sensitivity. As a result, we apply the following selection cuts:

- Azimuthal angle between the two leptons $|\Delta\phi(\ell_1, \ell_2)| \leq 1.9$

Signal Mass [GeV]	$N_{lepton} = 2$	Lepton Trigger	$N_b = 2$	$N_\tau < 2$	$N_Z = 1$	$N_h = 1$	$N_A = 1$
250	3.15e+4	3.14e+4	2.47e+3	2.47e+3	2.38e+3	1.73e+3	1.73e+3
300	6.6e+4	6.59e+4	6.24e+3	6.24e+3	6e+3	4.3e+3	4.3e+3
350	1.2e+3	1.2e+3	136	136	131	96.2	96.2
400	604	604	86.6	86.6	83.8	61.9	61.9
450	433	433	68.4	68.4	65.9	50.3	50.3
500	325	325	56.5	56.5	54.7	42.5	42.5
600	195	195	40.9	40.9	39.3	31.8	31.8
700	121	121	28	28	26.9	22	22
800	77.5	77.5	18.7	18.7	18	14.8	14.8
900	50.5	50.5	12.3	12.3	11.9	9.96	9.96
1000	33.9	33.8	7.55	7.55	7.31	5.98	5.98

Table 7: Expected number of pre-selected events for the $A \to Zh \to \ell\ell bb$ signal for $\int Ldt = 300$ fb^{-1} at $\sqrt{s} = 14$ TeV with $< N_{PU} >= 50$.

Background	$N_{lepton} = 2$	Lepton Trigger	$N_b = 2$	$N_\tau < 2$	$N_Z = 1$	$N_h = 1$	$N_A = 1$
B, Bj, Bjj-vbf, BB, BBB	4.58e+8	4.05e+8	1.15e+5	1.15e+5	9.91e+4	2.66e+4	2.66e+4
tj, tB, tt, ttB	7.53e+6	7.36e+6	8.31e+5	8.31e+5	5.69e+4	1.51e+4	1.51e+4
H	4.99e+4	4.48e+4	44.5	44.5	6.37	1.58	1.58
Total Background	4.65e+8	4.13e+8	9.47e+5	9.47e+5	1.56e+5	4.16e+4	4.16e+4

Table 8: Expected number of pre-selected events for the SM backgrounds to $A \to Zh \to \ell\ell bb$ for $\int Ldt = 300$ fb^{-1} at $\sqrt{s} = 14$ TeV with $< N_{PU} >= 50$.

Signal Mass [GeV]	$N_{lepton} = 2$	Lepton Trigger	$N_b = 2$	$N_\tau < 2$	$N_Z = 1$	$N_h = 1$	$N_A = 1$
250	1.29e+6	1.29e+6	5.44e+4	5.43e+4	5.07e+4	2.5e+4	2.5e+4
300	2.89e+6	2.89e+6	1.74e+5	1.74e+5	1.65e+5	8.47e+4	8.47e+4
350	5.64e+4	5.63e+4	4.31e+3	4.31e+3	4.1e+3	2.04e+3	2.04e+3
400	3.02e+4	3.02e+4	2.84e+3	2.84e+3	2.7e+3	1.38e+3	1.38e+3
450	2.3e+4	2.3e+4	2.56e+3	2.56e+3	2.46e+3	1.28e+3	1.28e+3
500	1.85e+4	1.85e+4	2.39e+3	2.39e+3	2.29e+3	1.25e+3	1.25e+3
600	1.23e+4	1.23e+4	1.98e+3	1.98e+3	1.9e+3	1.07e+3	1.07e+3
700	8.53e+3	8.52e+3	1.57e+3	1.57e+3	1.5e+3	893	893
800	5.98e+3	5.98e+3	1.14e+3	1.14e+3	1.1e+3	662	662
900	4.31e+3	4.31e+3	850	850	816	502	502
1000	3.11e+3	3.11e+3	569	568	546	325	325

Table 9: Expected number of pre-selected events for the $A \to Zh \to \ell\ell bb$ signal for $\int Ldt = 3000$ fb^{-1} at $\sqrt{s} = 33$ TeV with $< N_{PU} >= 140$.

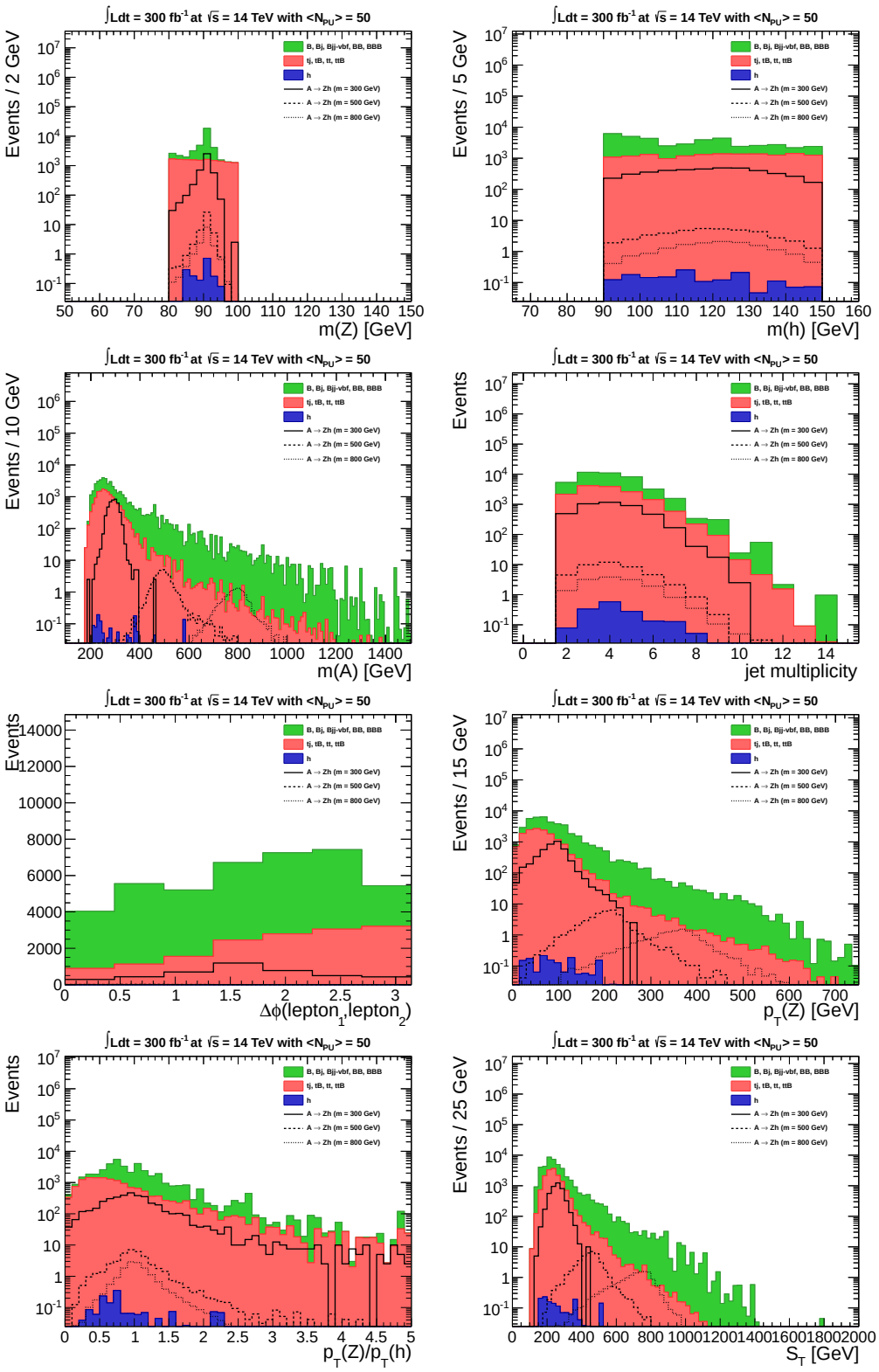


Figure 11: Kinematic distributions for pre-selected events in the bb channel, for $\int Ldt = 300$ fb^{-1} at $\sqrt{s} = 14$ TeV with $< N_{PU} >= 50$.

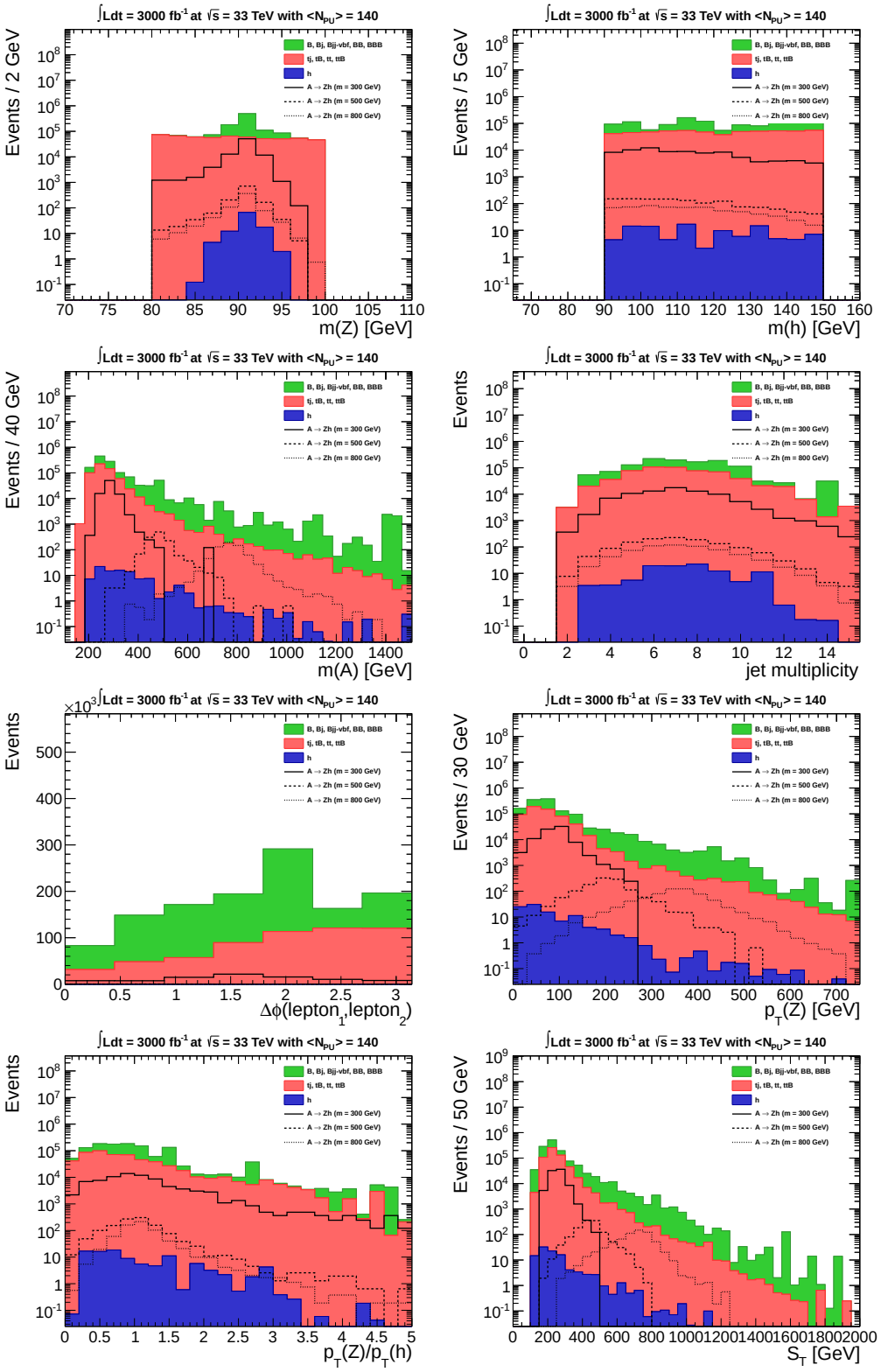


Figure 12: Kinematic distributions for pre-selected events in the bb channel, for $\int Ldt = 3000$ fb^{-1} at $\sqrt{s} = 33$ TeV with $< N_{PU} >= 140$.

Background	$N_{lepton} = 2$	Lepton Trigger	$N_b = 2$	$N_\tau < 2$	$N_Z = 1$	$N_h = 1$	$N_A = 1$
B, Bj, Bjj-vbf, BB, BBB	8.66e+9	7.68e+9	4.13e+6	4.13e+6	3.34e+6	6.68e+5	6.68e+5
tj, tB, tt, ttB	5.06e+8	4.86e+8	3.61e+7	3.61e+7	2.39e+6	5.81e+5	5.81e+5
H	2.21e+6	1.97e+6	2.54e+3	2.54e+3	370	103	103
Total Background	9.17e+9	8.17e+9	4.03e+7	4.03e+7	5.73e+6	1.25e+6	1.25e+6

Table 10: Expected number of pre-selected events for the SM backgrounds to $A \to Zh \to \ell\ell bb$ for $\int Ldt = 3000$ fb^{-1} at $\sqrt{s} = 33$ TeV with $< N_{PU} >= 140$.

- Transverse momentum of the Z candidate $p_T(Z) \geq 40$ GeV
- Ratio of the p_T of the Z and h candidates $0.4 \leq p_T(Z)/p_T(h) \leq 2.75$

The selected signal and background yields for the bb channel are shown in Tables 11 and 12 for the 300 fb^{-1}analysis at $\sqrt{s} = 14$ TeV, and Tables 13 and 14 for the 3000 fb^{-1}analysis at $\sqrt{s} = 33$ TeV. Analogous tables for the $\tau\tau$ channel are shown in Tables A.9, A.10, A.11, A.12. The m_A distributions for both channels are shown in Figure 13, for the analyses based on 300 fb^{-1} at $\sqrt{s} = 14$ TeV and 3000 fb^{-1} at $\sqrt{s} = 33$ TeV.

Signal Mass [GeV]	Pre-selection	$\lvert\Delta\phi(\ell_1\ell_2)\rvert \leq 1.9$	$p_T(Z) \geq 40$ GeV	$0.4 \leq \frac{p_T(Z)}{p_T(h)} \leq 2.75$
250	1.73e+3	544	529	447
300	4.3e+3	2.83e+3	2.82e+3	2.57e+3
350	96.2	77	76.9	72.4
400	61.9	54.6	54.6	52.1
450	50.3	46	46	43.6
500	42.5	40.3	40.3	38.4
600	31.8	31	31	30.1
700	22	21.7	21.7	21.3
800	14.8	14.7	14.7	14.4
900	9.96	9.91	9.91	9.76
1000	5.98	5.97	5.97	5.9

Table 11: Expected number of selected events for the $A \to Zh \to \ell\ell bb$ signal for $\int Ldt = 300$ fb^{-1} at $\sqrt{s} = 14$ TeV with $< N_{PU} >= 50$.

3.2.1 Results

The distribution of the A candidate invariant mass is used to assess discovery and exclusion potential. A 20% rate uncertainty in the backgrounds is assumed.

Figure A.3 shows the signal cross section required to exclude the $A \to Zh$ signal at 95% CL in both channels separately, and the combination, for $\int Ldt = 300$ fb^{-1} and 3000 fb^{-1} at $\sqrt{s} = 14$ TeV. Also shown is the cross section required for a 3σ and 5σ signal significance. Figure 14 overlays the signal cross sections required for exclusion

Background	Pre-selection	$\lvert\Delta\phi(\ell_1\ell_2)\rvert \leq 1.9$	$p_T(Z) \geq 40$ GeV	$0.4 \leq \frac{p_T(Z)}{p_T(h)} \leq 2.75$
B, Bj, Bjj-vbf, BB, BBB	2.66e+4	1.73e+4	7.92e+3	7.06e+3
tj, tB, tt, ttB	1.51e+4	6.68e+3	6.48e+3	5.78e+3
H	1.58	0.765	0.765	0.718
Total Background	4.16e+4	2.4e+4	1.44e+4	1.28e+4

Table 12: Expected number of selected events for the SM backgrounds to $A \to Zh \to \ell\ell bb$ for $\int Ldt = 300$ fb^{-1} at $\sqrt{s} = 14$ TeV with $< N_{PU} >= 50$.

Signal Mass [GeV]	Pre-selection	$\lvert\Delta\phi(\ell_1\ell_2)\rvert \leq 1.9$	$p_T(Z) \geq 40$ GeV	$0.4 \leq \frac{p_T(Z)}{p_T(h)} \leq 2.75$
250	2.5e+4	8.04e+3	7.98e+3	6.72e+3
300	8.47e+4	5.55e+4	5.53e+4	4.88e+4
350	2.04e+3	1.62e+3	1.62e+3	1.45e+3
400	1.38e+3	1.21e+3	1.21e+3	1.14e+3
450	1.28e+3	1.19e+3	1.19e+3	1.1e+3
500	1.25e+3	1.16e+3	1.16e+3	1.1e+3
600	1.07e+3	1.04e+3	1.04e+3	1e+3
700	893	881	881	851
800	662	659	659	646
900	502	499	499	491
1000	325	324	324	319

Table 13: Expected number of selected events for the $A \to Zh \to \ell\ell bb$ signal for $\int Ldt = 3000$ fb^{-1} at $\sqrt{s} = 33$ TeV with $< N_{PU} >= 140$.

Background	Pre-selection	$\lvert\Delta\phi(\ell_1\ell_2)\rvert \leq 1.9$	$p_T(Z) \geq 40$ GeV	$0.4 \leq \frac{p_T(Z)}{p_T(h)} \leq 2.75$
B, Bj, Bjj-vbf, BB, BBB	6.68e+5	4.38e+5	4.38e+5	4.16e+5
tj, tB, tt, ttB	5.81e+5	2.51e+5	2.44e+5	2.1e+5
H	103	46.8	46.8	17.5
Total Background	1.25e+6	6.89e+5	6.82e+5	6.26e+5

Table 14: Expected number of selected events for the SM backgrounds to $A \to Zh \to \ell\ell bb$ for $\int Ldt = 3000$ fb^{-1} at $\sqrt{s} = 33$ TeV with $< N_{PU} >= 140$.

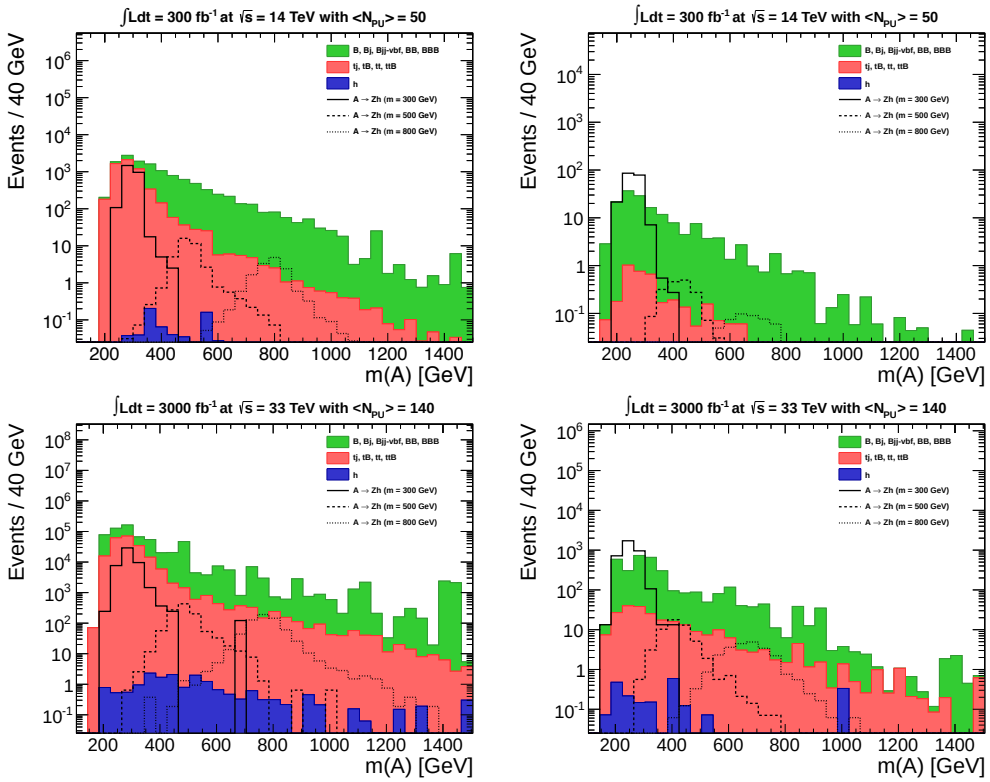


Figure 13: Distribution of the A candidate invariant mass in selected events for $\int Ldt = 300$ fb^{-1} at $\sqrt{s} = 14$ TeV with $< N_{PU} >= 50$ (top) and $\int Ldt = 3000$ fb^{-1} at $\sqrt{s} = 33$ TeV with $< N_{PU} >= 140$ (bottom). The bb ($\tau\tau$) channel is on the left (right).

or discovery based on the combination of the two channels, for various run conditions. These cross section limits are then interpreted in terms of the actual signal cross section for each point in parameter space, in order to determine discovery and exclusion potential for each mass hypothesis. Figure 15 shows the regions in the $\tan\beta$ versus $\cos(\beta-\alpha)$ plane which can be excluded at 95% CL for the three scenarios under consideration. Figures 16 and 17 show the masses for which 3σ and 5σ significance can be obtained in the $\tan(\beta)$ versus $\cos(\beta-\alpha)$ plane. Once again, direct search limits provide considerable complementarity to Higgs coupling measurements [25]. In this case, the direct search limits weaken only at large $\tan(\beta)$ where the production cross section for A falls due to diminishing coupling to the top quark, as well as close to the alignment limit $|\cos(\beta-\alpha)| \to 0$ where the branching ratio for $A \to Zh$ vanishes.

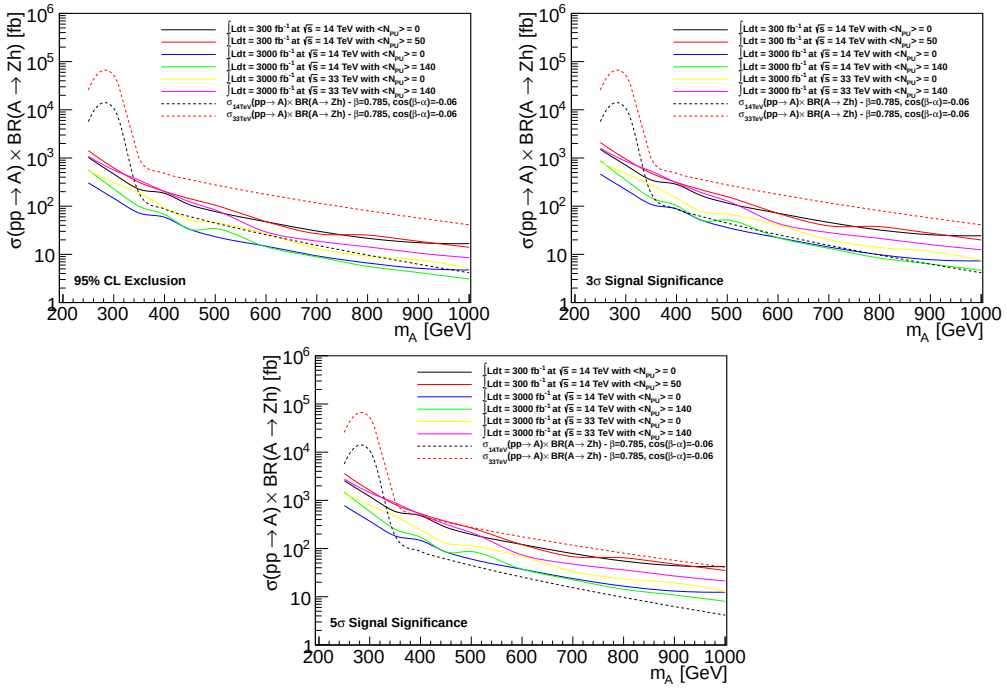


Figure 14: The cross section which can be excluded at 95% CL, and the cross section required for a 3σ and 5σ signal significance, as a function of the A mass.

4 Conclusion

Searches for extended Higgs sectors at future colliders are extremely well motivated. We have analyzed the sensitivity of direct searches for heavy, neutral Higgs bosons at future hadron colliders with $\sqrt{s} = 14$ TeV and $\sqrt{s} = 33$ TeV. The potential to either exclude or discover an extended Higgs sector is found to significantly exceed existing exclusion limits, and probe regions of parameter space which can't be constrained by precision measurements of the SM-like Higgs boson couplings. The complementarity between direct search and precision measurement is a key finding of this analysis; the exploitation of which will allow, at future hadron colliders, exclusion or discovery of additional neutral Higgs scalars or pseudoscalars with a mass of 300 GeV, for values of

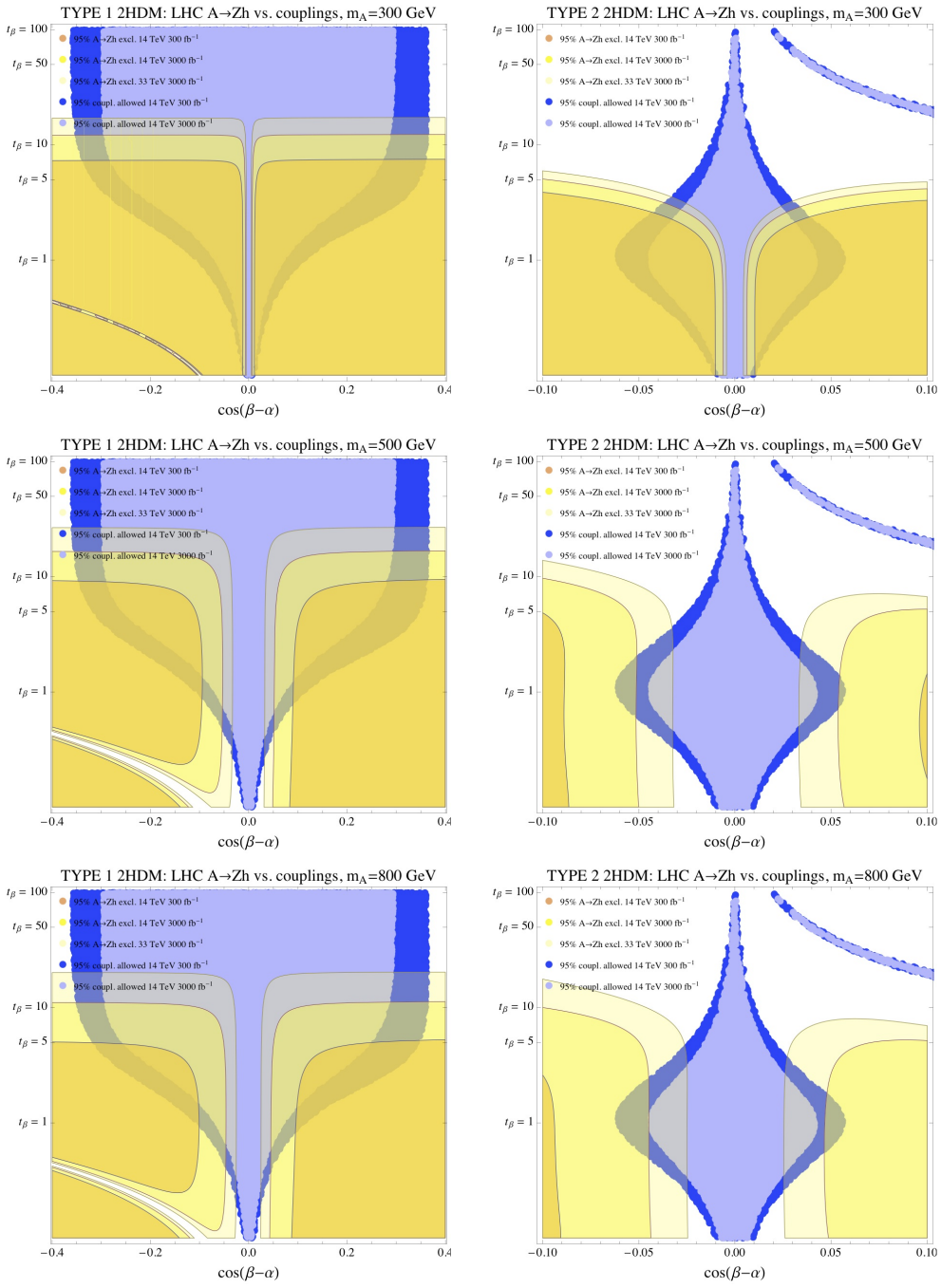


Figure 15: The region of parameter space which could be excluded at 95% CL for various A mass hypotheses in a type I (left) and type II (right) 2HDM. The dark yellow region corresponds to 300 fb^{-1} at $\sqrt{s} = 14$ TeV, the yellow region to 3000 fb^{-1} at $\sqrt{s} = 14$ TeV, and the light yellow region to 3000 fb^{-1} at $\sqrt{s} = 33$ TeV. The region which would remain allowed at 95% CL based on non-observation of deviations from the SM in precision Higgs coupling measurements is shown in dark (light) blue for 300 fb^{-1} (3000 fb^{-1}) [25].

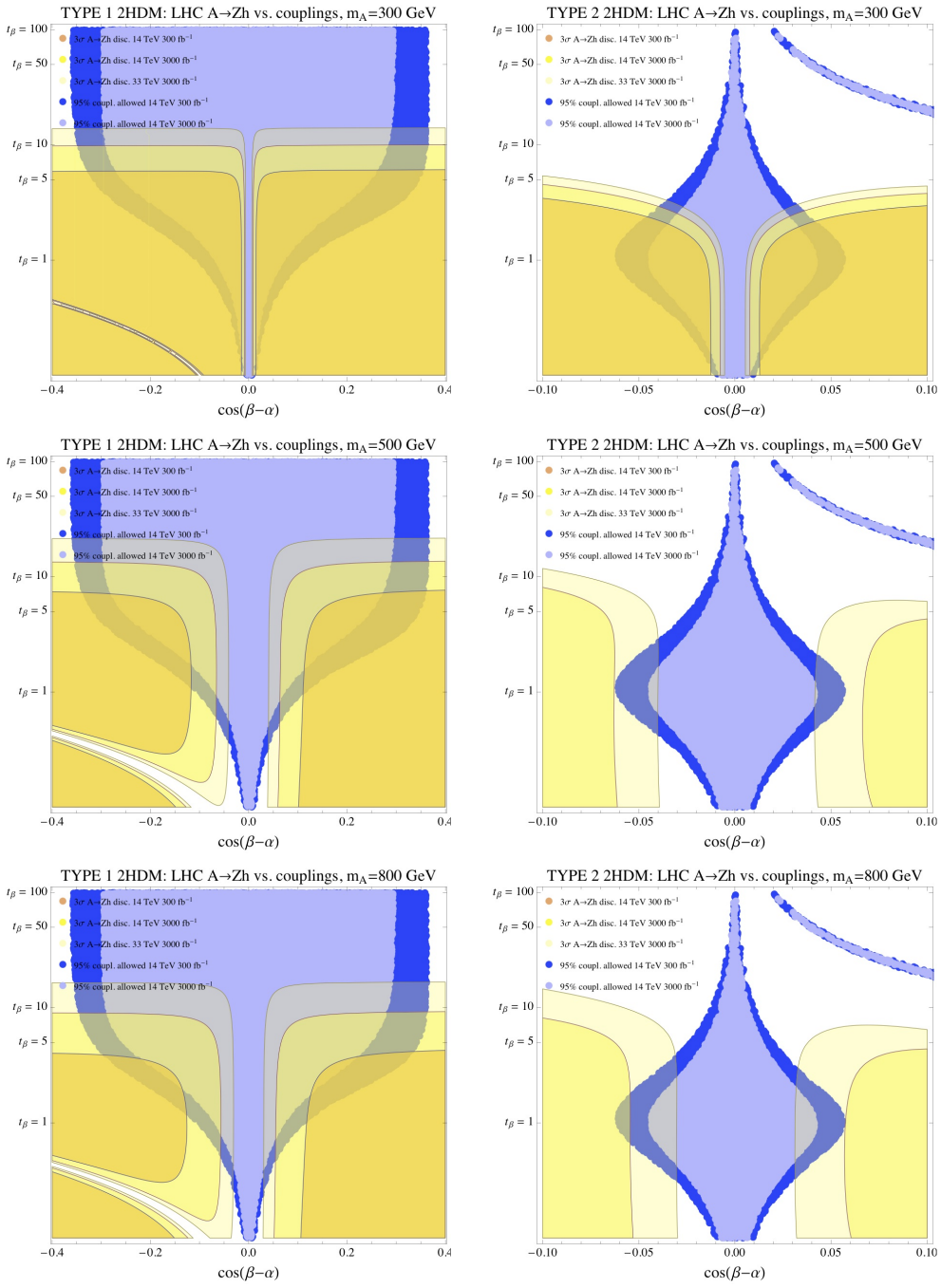


Figure 16: The region of parameter space for which a 3σ signal significance could be obtained for various A mass hypotheses in a type I (left) and type II (right) 2HDM. The dark yellow region corresponds to 300 fb^{-1} at $\sqrt{s} = 14$ TeV, the yellow region to 3000 fb^{-1} at $\sqrt{s} = 14$ TeV, and the light yellow region to 3000 fb^{-1} at $\sqrt{s} = 33$ TeV. The region which would remain allowed at 95% CL based on non-observation of deviations from the SM in precision Higgs coupling measurements is shown in dark (light) blue for 300 fb^{-1} (3000 fb^{-1}) [25].

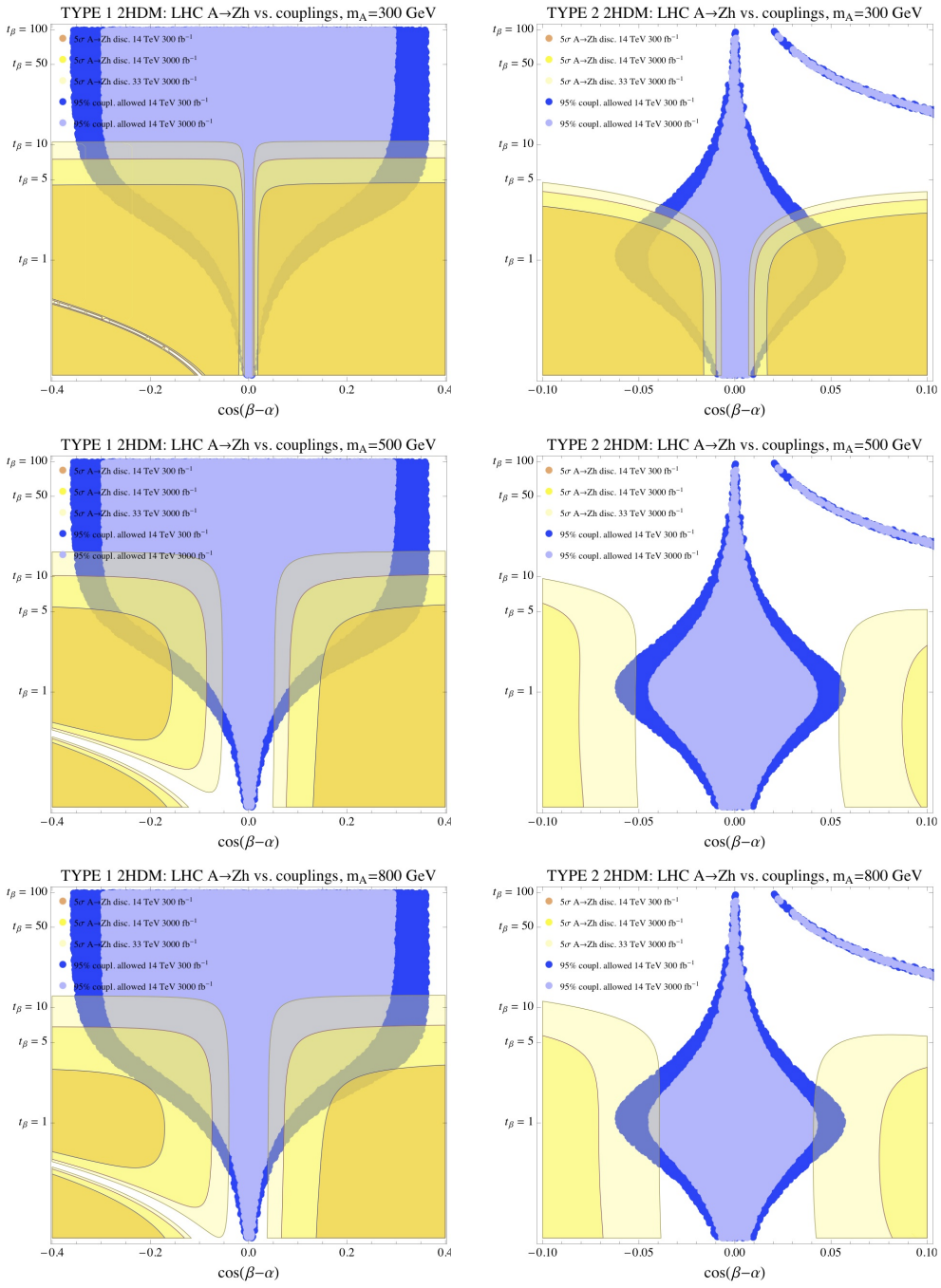


Figure 17: The region of parameter space for which a 5σ signal significance could be obtained for various A mass hypotheses in a type I (left) and type II (right) 2HDM. The dark yellow region corresponds to 300 fb^{-1} at $\sqrt{s} = 14$ TeV, the yellow region to 3000 fb^{-1} at $\sqrt{s} = 14$ TeV, and the light yellow region to 3000 fb^{-1} at $\sqrt{s} = 33$ TeV. The region which would remain allowed at 95% CL based on non-observation of deviations from the SM in precision Higgs coupling measurements is shown in dark (light) blue for 300 fb^{-1} (3000 fb^{-1}) [25].

$|\cos(\beta-\alpha)|$ as small as ~ 0.01 with $\tan(\beta) \lesssim 1$, in both type I and II 2HDMs. The results are compared with and without the addition of additional minimum bias events, and found to be robust against pileup.

References

[1] S. Chatrchyan et al., "Observation of a new boson at a mass of 125 GeV with the CMS experiment at the LHC", *Phys. Lett. B* **716** (Jul, 2012) 30–61. 59 p.

[2] G. Aad et al., "Observation of a new particle in the search for the Standard Model Higgs boson with the ATLAS detector at the LHC", *Physics Letters B* **716** (2012), no. 1, 1 – 29, doi:http://dx.doi.org/10.1016/j.physletb.2012.08.020.

[3] T. D. Lee, "A Theory of Spontaneous T Violation", *Phys. Rev. D* **8** (Aug, 1973) 1226–1239, doi:10.1103/PhysRevD.8.1226.

[4] G. Branco et al., "Theory and phenomenology of two-Higgs-doublet models", *Phys.Rept.* **516** (2012) 1–102, doi:10.1016/j.physrep.2012.02.002, arXiv:1106.0034.

[5] S. Dimopoulos and H. Georgi, "Softly broken supersymmetry and SU(5)", *Nuclear Physics B* **193** (1981), no. 1, 150 – 162, doi:http://dx.doi.org/10.1016/0550-3213(81)90522-8.

[6] H. Haber and G. Kane, "The search for supersymmetry: Probing physics beyond the standard model", *Physics Reports* **117** (1985), no. 2–4, 75 – 263, doi:http://dx.doi.org/10.1016/0370-1573(85)90051-1.

[7] Z. Chacko et al., "Natural little hierarchy from a partially goldstone twin Higgs", *JHEP* **0601** (2006) 126, doi:10.1088/1126-6708/2006/01/126, arXiv:hep-ph/0510273.

[8] Z. Chacko, H.-S. Goh, and R. Harnik, "The Twin Higgs: Natural electroweak breaking from mirror symmetry", *Phys.Rev.Lett.* **96** (2006) 231802, doi:10.1103/PhysRevLett.96.231802, arXiv:hep-ph/0506256.

[9] J. Mrazek et al., "The Other Natural Two Higgs Doublet Model", *Nucl.Phys.* **B853** (2011) 1–48, doi:10.1016/j.nuclphysb.2011.07.008, arXiv:1105.5403.

[10] D. B. Kaplan and H. Georgi, "SU(2) U(1) breaking by vacuum misalignment", *Physics Letters B* **136** (1984), no. 3, 183 – 186, doi:http://dx.doi.org/10.1016/0370-2693(84)91177-8.

[11] K. Agashe, R. Contino, and A. Pomarol, "The Minimal composite Higgs model", *Nucl.Phys.* **B719** (2005) 165–187, doi:10.1016/j.nuclphysb.2005.04.035, arXiv:hep-ph/0412089.

[12] "Combination of standard model Higgs boson searches and measurements of the properties of the new boson with a mass near 125 GeV", Technical Report CMS-PAS-HIG-13-005, CERN, Geneva, (2013).

[13] "Combined coupling measurements of the Higgs-like boson with the ATLAS detector using up to 25 fb^{-1} of proton-proton collision data", Technical Report ATLAS-CONF-2013-034, CERN, Geneva, (Mar, 2013).

[14] N. Craig, J. Galloway, and S. Thomas, "Searching for Signs of the Second Higgs Doublet", arXiv:1305.2424.

[15] C.-Y. Chen and S. Dawson, "Exploring Two Higgs Doublet Models Through Higgs Production", doi:10.1103/PhysRevD.87.055016, arXiv:1301.0309.

[16] C.-Y. Chen, S. Dawson, and M. Sher, "Heavy Higgs Searches and Constraints on Two Higgs Doublet Models", *Phys.Rev.* **D88** (2013) 015018, doi:10.1103/PhysRevD.88.015018, arXiv:1305.1624.

[17] C.-Y. Chen, "Projections for Two Higgs Doublet Models at the LHC and ILC: A Snowmass White Paper", arXiv:1308.3487.

[18] A. Avetisyan et al., "Methods and Results for Standard Model Event Generation at $\sqrt{s} = 14$ TeV, 33 TeV and 100 TeV Proton Colliders (A Snowmass Whitepaper)", arXiv:1308.1636.

[19] A. Avetisyan et al., "Snowmass Energy Frontier Simulations using the Open Science Grid (A Snowmass 2013 whitepaper)", arXiv:1308.0843.

[20] J. Alwall et al., "MadGraph 5 : Going Beyond", *JHEP* **1106** (2011) 128, doi:10.1007/JHEP06(2011)128, arXiv:1106.0522.

[21] T. Sjostrand, S. Mrenna, and P. Z. Skands, "PYTHIA 6.4 Physics and Manual", *JHEP* **0605** (2006) 026, doi:10.1088/1126-6708/2006/05/026, arXiv:hep-ph/0603175.

[22] J. de Favereau et al., "DELPHES 3, A modular framework for fast simulation of a generic collider experiment", arXiv:1307.6346.

[23] J. Anderson et al., "Snowmass Energy Frontier Simulations", arXiv:1309.1057.

[24] R. V. Harlander and W. B. Kilgore, "Next-to-next-to-leading order Higgs production at hadron colliders", *Phys.Rev.Lett.* **88** (2002) 201801, doi:10.1103/PhysRevLett.88.201801, arXiv:hep-ph/0201206.

[25] V. Barger et al., "Scrutinizing h(125) in Two Higgs Doublet Models at the LHC, ILC, and Muon Collider", arXiv:1308.0052.

5 Appendix

Mass [GeV]	Cross Section [fb]	Branching Ratio
200	2.41e+4	0.128
250	1.62e+4	0.196
300	1.27e+4	0.0915
350	1.32e+4	0.0411
400	1.2e+4	0.00558
450	8.53e+3	0.00423
500	5.74e+3	0.00414
600	2.55e+3	0.00486
700	1.19e+3	0.00614
800	580	0.00785
900	299	0.01
1000	161	0.0127

Table A.1: Cross section and branching ratio for $pp \to H \to ZZ$ at $\sqrt{s} = 14$ TeV in a type II 2HDM for the benchmark point with $\cos(\beta - \alpha) = -0.06$ and $\tan(\beta) = 1$.

Mass [GeV]	Cross Section [fb]	Branching Ratio
250	3.7e+4	0.154
300	3.37e+4	0.318
350	5.98e+4	0.00308
400	3.08e+4	0.00284
450	1.69e+4	0.00359
500	9.77e+3	0.00456
600	3.67e+3	0.00696
700	1.55e+3	0.00993
800	718	0.0135
900	356	0.0176
1000	187	0.0222

Table A.2: Cross section and branching ratio for $pp \to A \to Zh$ at $\sqrt{s} = 14$ TeV in a type II 2HDM for the benchmark point with $\cos(\beta - \alpha) = -0.06$ and $\tan(\beta) = 1$.

Mass [GeV]	Cross Section [fb]	Branching Ratio
200	1.01e+5	0.128
250	7.35e+4	0.196
300	6.15e+4	0.0915
350	6.87e+4	0.0411
400	6.63e+4	0.00558
450	5e+4	0.00423
500	3.55e+4	0.00414
600	1.76e+4	0.00486
700	8.98e+3	0.00614
800	4.83e+3	0.00785
900	2.73e+3	0.01
1000	1.6e+3	0.0127

Table A.3: Cross section and branching ratio for $pp \to H \to ZZ$ at $\sqrt{s} = 33$ TeV in a type II 2HDM for the benchmark point with $\cos(\beta - \alpha) = -0.06$ and $\tan(\beta) = 1$.

Mass [GeV]	Cross Section [fb]	Branching Ratio
250	1.68e+5	0.154
300	1.64e+5	0.318
350	3.11e+5	0.00308
400	1.7e+5	0.00284
450	9.91e+4	0.00359
500	6.05e+4	0.00456
600	2.52e+4	0.00696
700	1.18e+4	0.00993
800	5.97e+3	0.0135
900	3.24e+3	0.0176
1000	1.85e+3	0.0222

Table A.4: Cross section and branching ratio for $pp \to A \to Zh$ at $\sqrt{s} = 33$ TeV in a type II 2HDM for the benchmark point with $\cos(\beta - \alpha) = -0.06$ and $\tan(\beta) = 1$.

Signal Mass [GeV]	$N_{lepton} = 2$	Lepton Trigger	$N_\tau = 2$	$N_b < 2$	$N_Z = 1$	$N_h = 1$	$N_A = 1$
250	3.28e+3	3.25e+3	221	221	210	176	176
300	6.47e+3	6.44e+3	471	471	453	377	377
350	114	114	9.02	9	8.52	6.9	6.9
400	55.1	54.9	4.67	4.67	4.45	3.64	3.64
450	39	38.9	3.67	3.66	3.51	2.81	2.81
500	28.5	28.5	2.79	2.78	2.66	2.13	2.13
600	16.6	16.6	1.77	1.77	1.68	1.28	1.28
700	9.9	9.89	1.18	1.18	1.12	0.874	0.874
800	6.21	6.21	0.775	0.774	0.74	0.568	0.568
900	4	4	0.521	0.521	0.498	0.388	0.388
1000	2.63	2.62	0.332	0.332	0.317	0.243	0.243

Table A.5: Expected number of pre-selected events for the $A \to Zh \to \ell\ell\tau\tau$ signal for $\int Ldt = 300$ fb^{-1} at $\sqrt{s} = 14$ TeV with $< N_{PU} >= 50$.

Background	$N_{lepton} = 2$	Lepton Trigger	$N_\tau = 2$	$N_b < 2$	$N_Z = 1$	$N_h = 1$	$N_A = 1$
B, Bj, Bjj-vbf, BB, BBB	4.58e+8	4.05e+8	1.9e+3	1.9e+3	701	399	399
tj, tB, tt, ttB	7.53e+6	7.36e+6	2.49e+3	2.43e+3	30.2	8.92	8.92
H	4.99e+4	4.48e+4	5.13	5.13	1.33	0.384	0.384
Total Background	4.65e+8	4.13e+8	4.4e+3	4.33e+3	732	408	408

Table A.6: Expected number of pre-selected events for the SM backgrounds to $A \to Zh \to \ell\ell\tau\tau$ for $\int Ldt = 300$ fb^{-1} at $\sqrt{s} = 14$ TeV with $< N_{PU} >= 50$.

Signal Mass [GeV]	$N_{lepton} = 2$	Lepton Trigger	$N_\tau = 2$	$N_b < 2$	$N_Z = 1$	$N_h = 1$	$N_A = 1$
250	1.3e+5	1.29e+5	5.14e+3	5.14e+3	4.65e+3	3.16e+3	3.16e+3
300	2.82e+5	2.8e+5	1.22e+4	1.22e+4	1.13e+4	7.25e+3	7.25e+3
350	5.38e+3	5.36e+3	290	290	266	173	173
400	2.81e+3	2.8e+3	156	156	143	93.6	93.6
450	2.08e+3	2.07e+3	133	132	122	72	72
500	1.64e+3	1.64e+3	118	118	111	67	67
600	1.07e+3	1.07e+3	87	86.9	82	46.7	46.7
700	714	713	65.3	65.2	61.6	36.4	36.4
800	494	493	50.6	50.5	47.7	27.1	27.1
900	348	348	35.8	35.7	33.7	18.6	18.6
1000	249	248	26.3	26.2	24.9	14.1	14.1

Table A.7: Expected number of pre-selected events for the $A \to Zh \to \ell\ell\tau\tau$ signal for $\int Ldt = 3000$ fb^{-1} at $\sqrt{s} = 33$ TeV with $< N_{PU} >= 140$.

Background	$N_{lepton} = 2$	Lepton Trigger	$N_\tau = 2$	$N_b < 2$	$N_Z = 1$	$N_h = 1$	$N_A = 1$
B, Bj, Bjj-vbf, BB, BBB	8.66e+9	7.68e+9	1.6e+6	1.6e+6	1.43e+6	9.75e+3	9.75e+3
tj, tB, tt, ttB	5.06e+8	4.86e+8	3.9e+5	3.78e+5	1.97e+4	610	609
H	2.21e+6	1.97e+6	791	790	102	37.4	37.4
Total Background	9.17e+9	8.17e+9	1.99e+6	1.98e+6	1.45e+6	1.04e+4	1.04e+4

Table A.8: Expected number of pre-selected events for the SM backgrounds to $A \to Zh \to \ell\ell\tau\tau$ for $\int Ldt = 3000$ fb^{-1} at $\sqrt{s} = 33$ TeV with $< N_{PU} >= 140$.

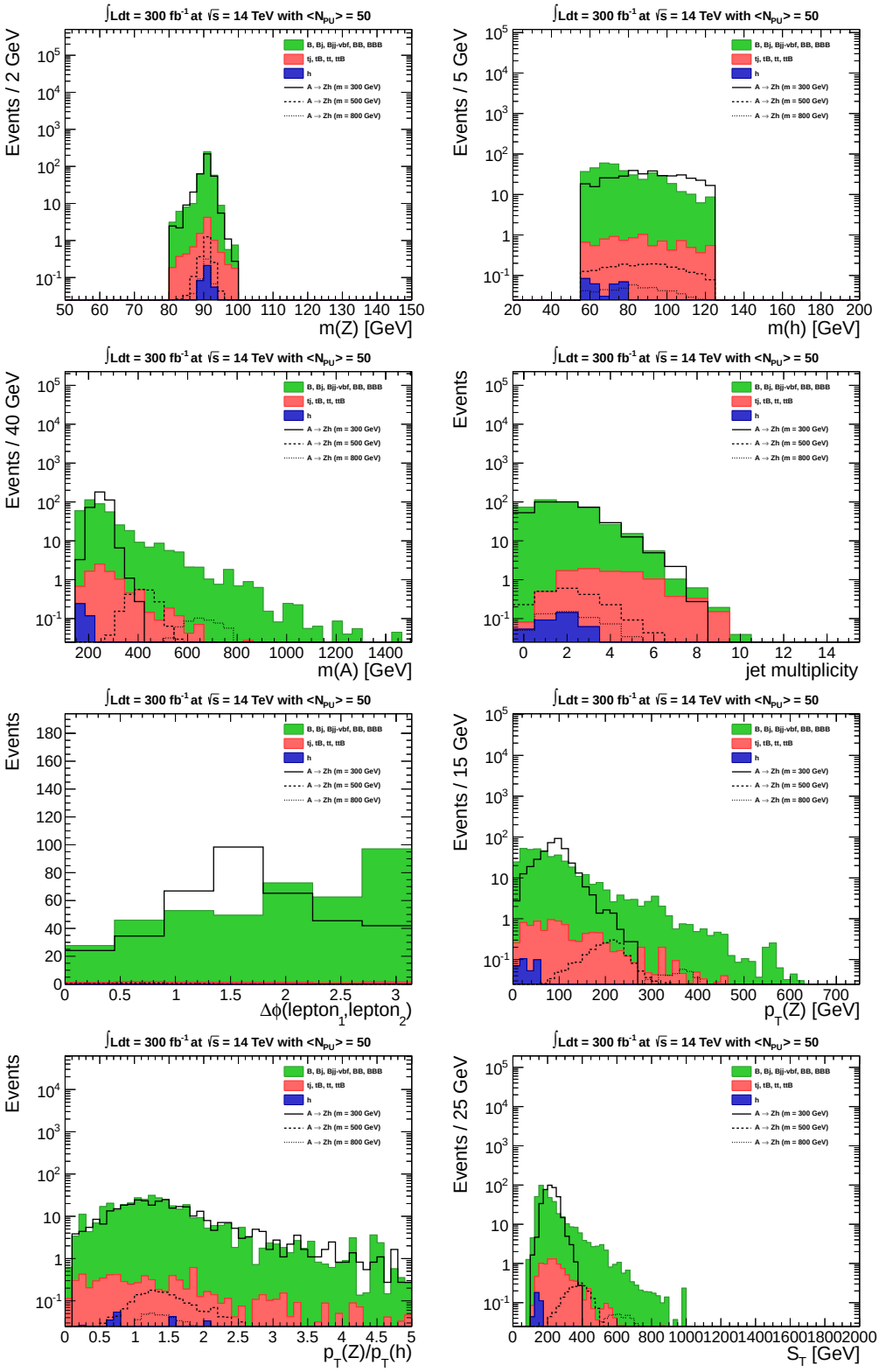


Figure A.1: Kinematic distributions for pre-selected events in the $\tau\tau$ channel, for $\int Ldt = 300$ fb^{-1} at $\sqrt{s} = 14$ TeV with $< N_{PU} >= 50$.

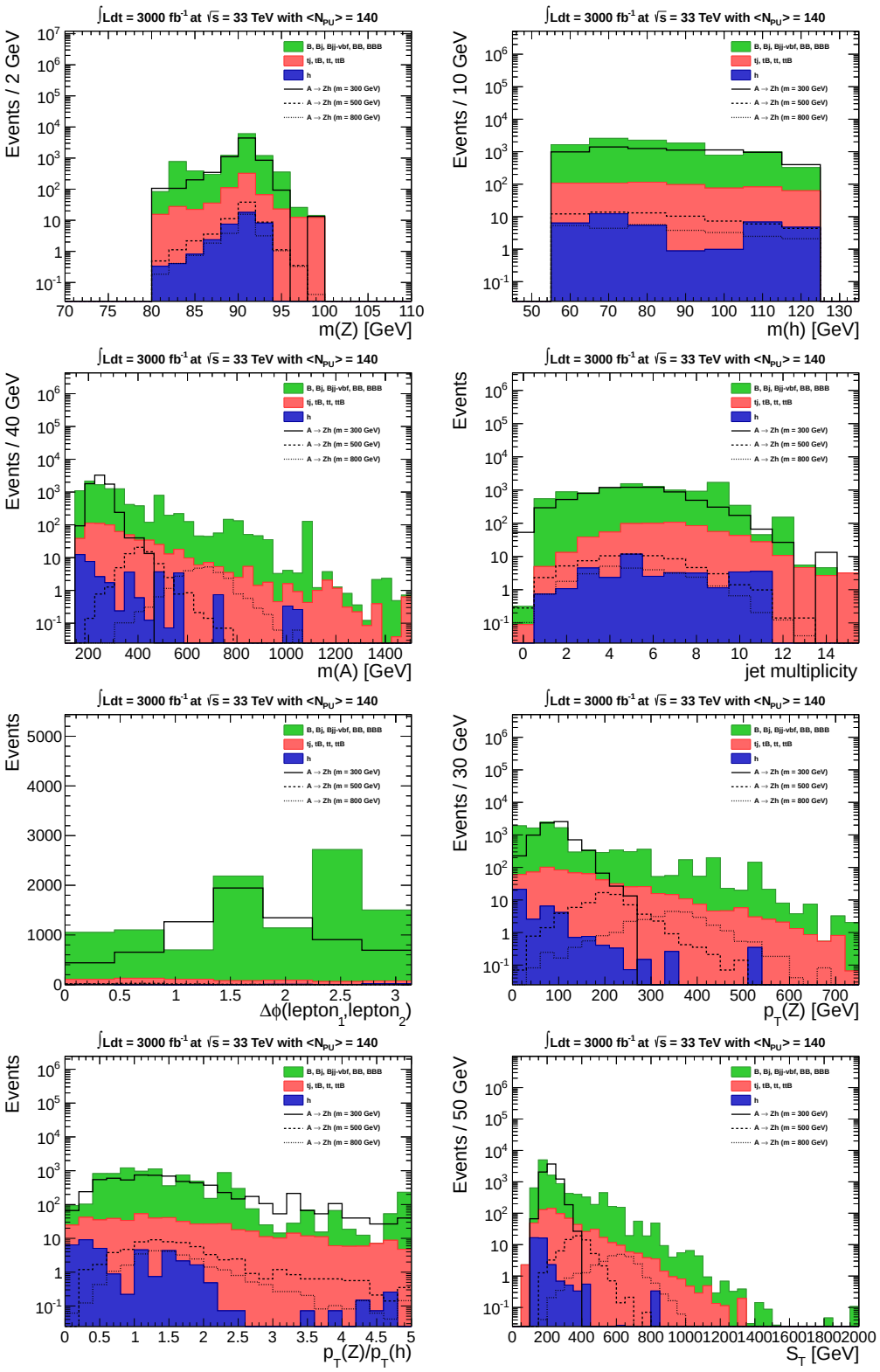


Figure A.2: Kinematic distributions for pre-selected events in the $\tau\tau$ channel, for $\int Ldt = 3000$ fb^{-1} at $\sqrt{s} = 33$ TeV with $< N_{PU} >= 140$.

Signal Mass [GeV]	Pre-selection	$\lvert\Delta\phi(\ell_1\ell_2)\rvert \leq 1.9$	$p_T(Z) \geq 40$ GeV	$0.4 \leq \frac{p_T(Z)}{p_T(h)} \leq 2.75$
250	176	54.8	52.2	38.7
300	377	240	239	194
350	6.9	5.42	5.42	4.57
400	3.64	3.13	3.13	2.74
450	2.81	2.55	2.55	2.22
500	2.13	2.02	2.01	1.77
600	1.28	1.24	1.24	1.13
700	0.874	0.855	0.855	0.787
800	0.568	0.564	0.564	0.52
900	0.388	0.385	0.385	0.358
1000	0.243	0.242	0.242	0.228

Table A.9: Expected number of selected events for the $A \to Zh \to \ell\ell\tau\tau$ signal for $\int Ldt = 300$ fb^{-1} at $\sqrt{s} = 14$ TeV with $< N_{PU} >= 50$.

Background	Pre-selection	$\lvert\Delta\phi(\ell_1\ell_2)\rvert \leq 1.9$	$p_T(Z) \geq 40$ GeV	$0.4 \leq \frac{p_T(Z)}{p_T(h)} \leq 2.75$
B, Bj, Bjj-vbf, BB, BBB	399	190	185	153
tj, tB, tt, ttB	8.92	6.02	6	3.66
H	0.384	0.0233	0.0233	0.0163
Total Background	408	196	191	157

Table A.10: Expected number of selected events for the SM backgrounds to $A \to Zh \to \ell\ell\tau\tau$ for $\int Ldt = 300$ fb^{-1} at $\sqrt{s} = 14$ TeV with $< N_{PU} >= 50$.

Signal Mass [GeV]	Pre-selection	$\lvert\Delta\phi(\ell_1\ell_2)\rvert \leq 1.9$	$p_T(Z) \geq 40$ GeV	$0.4 \leq \frac{p_T(Z)}{p_T(h)} \leq 2.75$
250	3.16e+3	1.01e+3	980	671
300	7.25e+3	4.58e+3	4.58e+3	3.54e+3
350	173	135	135	110
400	93.6	81.7	81.6	68.5
450	72	65.8	65.8	56.6
500	67	62.6	62.6	53.5
600	46.7	45	45	39
700	36.4	35.5	35.5	31.6
800	27.1	26.6	26.6	24.2
900	18.6	18.5	18.5	16.7
1000	14.1	14	14	12.7

Table A.11: Expected number of selected events for the $A \to Zh \to \ell\ell\tau\tau$ signal for $\int Ldt = 3000$ fb^{-1} at $\sqrt{s} = 33$ TeV with $< N_{PU} >= 140$.

Background	Pre-selection	$\lvert\Delta\phi(\ell_1\ell_2)\rvert \leq 1.9$	$p_T(Z) \geq 40$ GeV	$0.4 \leq \frac{p_T(Z)}{p_T(h)} \leq 2.75$
B, Bj, Bjj-vbf, BB, BBB	9.75e+3	4.7e+3	4.7e+3	3.12e+3
tj, tB, tt, ttB	609	431	429	241
H	37.4	3.54	3.54	2.25
Total Background	1.04e+4	5.14e+3	5.13e+3	3.36e+3

Table A.12: Expected number of selected events for the SM backgrounds to $A \to Zh \to \ell\ell\tau\tau$ for $\int Ldt = 3000$ fb^{-1} at $\sqrt{s} = 33$ TeV with $< N_{PU} >= 140$.

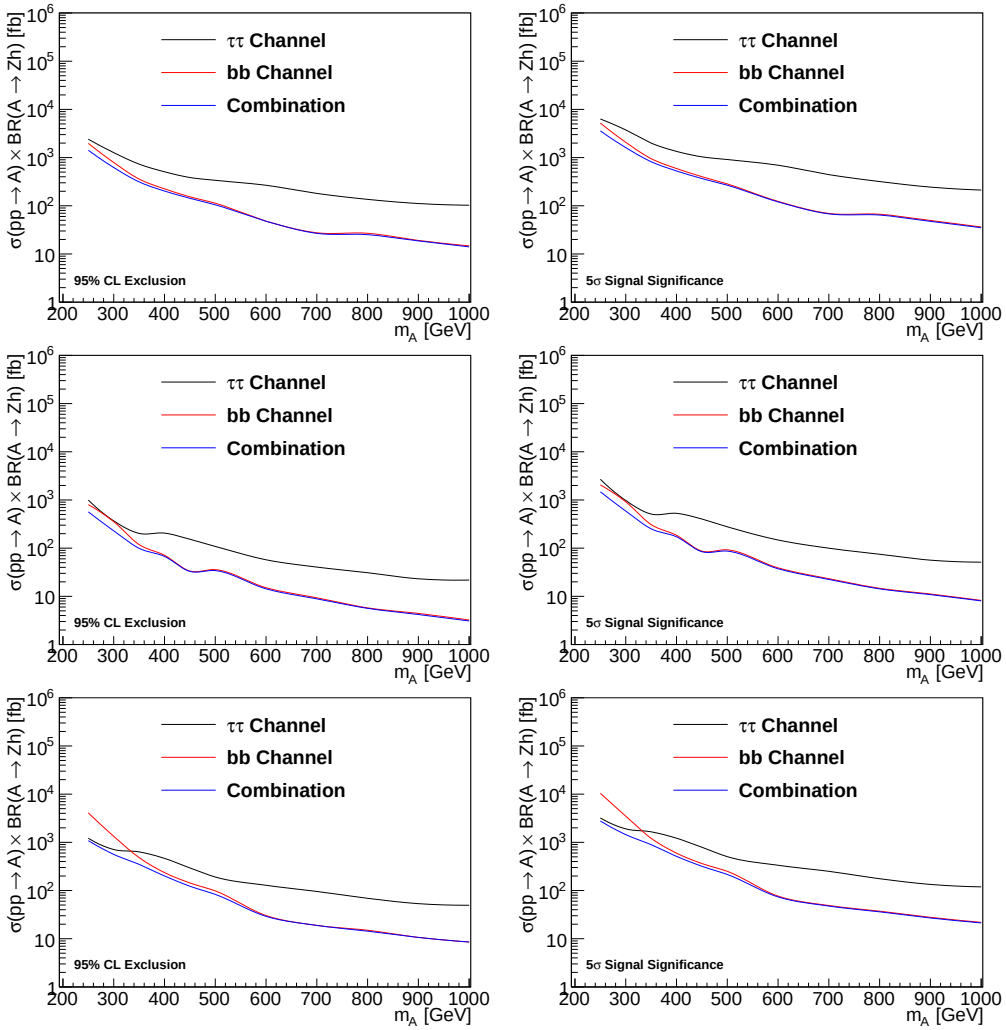


Figure A.3: The cross section which can be excluded at 95% CL (left) and the cross section required for a 5σ signal significance (right), for each A mass hypothesis. The bb and $\tau\tau$ channels are shown separately, as well as the combination. The top row shows results for $\int Ldt = 300$ fb^{-1} at $\sqrt{s} = 14$ TeV with $< N_{PU} >= 50$, the middle row for $\int Ldt = 3000$ fb^{-1} at $\sqrt{s} = 14$ TeV with $< N_{PU} >= 140$, and the bottom row for $\int Ldt = 3000$ fb^{-1} at $\sqrt{s} = 33$ TeV with $< N_{PU} >= 140$.